Uniform electric-field-induced non-Newtonian rheology of a dilute suspension of deformable Newtonian drops

Shubhadeep Mandal and Suman Chakraborty*
Department of Mechanical Engineering, Indian Institute of Technology Kharagpur, Kharagpur, West Bengal 721302, India
(Received 27 March 2017; published 14 September 2017)

The rheological behavior of a dilute emulsion comprised of neutrally buoyant drops suspended in an immiscible medium under the combined influence of a uniform electric field and simple shear flow is analyzed. Considering the drops and suspending medium as Newtonian and leaky dielectrics, the effective emulsion stress tensor is obtained when the fluid motion is governed by the Stokes equations. The present study takes into account an arbitrarily oriented uniform electric field in the plane of shear flow. A small-deformation analysis is performed to study this coupled electrohydrodynamic problem considering weak imposed shear flow and weak surface charge convection. Analytical expressions are obtained for the effective shear viscosity and normal stress differences of the dilute emulsion. The tilt angle (orientation angle of the applied electric field relative to the direction of shear flow) is found to affect the emulsion rheology. Key results show that the dilute emulsion exhibits non-Newtonian behavior such as shear-rate-dependent effective viscosity and nonzero first and second normal stress differences. In the absence of shape deformation and charge convection, a dilute emulsion displays shear thinning or shear thickening behavior depending on the drop polarization and tilt angle. The effective viscosity of the dilute emulsion can be lower or higher than the viscosity of the suspending medium depending on the electrical property ratios, tilt angle, and relative strength of the electric stress as compared with viscous stress. Surface charge convection significantly affects the electrohydrodynamic flow and thereby modifies the effective viscosity and normal stress differences. The applied electric field significantly affects the drop shape and orientation angle and thereby modifies the effective viscosity and normal stress differences. Both the surface charge convection and shape deformation can increase or decrease the effective viscosity and normal stress differences. Notably, the presence of surface charge convection and shape deformation leads to the generation of electric torque, which further results in a nonzero antisymmetric component of the emulsion stress tensor. We establish that fine-tuned rheology of a dilute emulsion can be obtained by proper choices of the tilt angle.

DOI: 10.1103/PhysRevFluids.2.093602

I. INTRODUCTION

Rheological behavior of complex fluids or soft matters is of immense interest to science and engineering communities not only due to remarkable rheological properties exhibited by these materials, but also attributed to far-ranging applications in chemical, biochemical, and pharmaceutical industries [1–3]. In these applications, it is common to have emulsions (comprised of immiscible dispersed liquid drops in a continuous liquid phase) that show complex flow characteristics in response to external stresses [4]. The macroscopic rheological properties of such emulsions depend not only on the emulsification process but also on the distribution of drops, size of drops, morphology of drops, and drop-drop interactions [5,6]. Understanding the relationship among these controlling factors is of prime importance for the design and performance of emulsifiers. The

*suman@mech.iitkgp.ernet.in

electric field, in this regard, is one of the promising external effects that can be used to alter or manipulate the emulsion rheology [7].

Starting from the seminal work of Taylor [8,9] on the effective viscosity of dilute emulsion, remarkable effort has been dedicated to understanding the relation between drop-level flow dynamics and macroscopic rheological properties. Taylor [8] has studied the hydrodynamics of a neutrally buoyant Newtonian drop suspended in another Newtonian fluid undergoing a simple shear flow. When the shear flow is weak, Taylor obtained that the imposed shear flow deforms the drop into an ellipsoidal shape and the major axis of the ellipsoid makes an angle of $\pi/4$ with the shear flow direction. The presence of the drop perturbs or modifies the imposed shear flow around itself, which yields a rheology of a dilute emulsion that is different from the rheological behavior of suspending fluid. Neglecting the shape deformation, Taylor obtained that the dilute emulsion behaves as a Newtonian fluid but with increased effective viscosity as compared with the viscosity of the suspending fluid. Incorporating the effects of shape deformation, Schowalter *et al.* [10] showed that the dilute emulsion exhibits elastic properties such as normal stress differences, which are generally characteristic of viscoelastic fluids. Later, several authors investigated theoretically and experimentally the emulsion rheology in the presence of inertia [11,12], viscoelasticity [13], surfactant [14,15], and interfacial slip [16,17] (refer to the works of Faroughi and Huber [18] and Pal [19,20] for more detail reviews) for both dilute and concentrated emulsions.

External uniform electric fields have been shown to manipulate the emulsion rheology [21–23]. Application of a uniform electric field not only alters the drop shape but also induces electrohydrodynamic (EHD) straining flow [24]. Thus, in the combined presence of a uniform electric field and shear flow, the relative strength of the electric field as compared with the shear rate will strongly influence the drop shape, orientation, and flow field [25], which in turn will affect the emulsion rheology. The effect of a uniform electric field acting in the direction of the velocity gradient was studied experimentally for a concentrated emulsion in shear flow [22]. Interesting observations were made by Ha and Yang [22], who investigated the rheology of oil-in-oil emulsions when the electrical conductivity of the drop phase is smaller than the suspending phase. They measured that the effective viscosity of the emulsion can be larger or smaller than the viscosity of the suspending medium depending on the relative magnitude of electric and viscous stresses and electrical properties of the oils. Fernandez [26–28] has performed numerical simulations and obtained similar rheological behavior. Vlahovska [29] has given a theory for the dilute emulsion in the combined presence of a uniform electric field and shear flow for two different cases: (i) highly viscous drops and (ii) weak flow. A small-deformation analysis for highly viscous drops that incorporates effects of shape deformation and charge convection shows that the dilute emulsion exhibits shear thinning or thickening behavior and normal stress differences. In the weak-flow limit, the emulsion rheology is only obtained up to leading order, which shows that the electric field does not affect the effective viscosity but induces normal stress differences [29]. In a recent study we investigated the pivotal role of shape deformation and charge convection on the uniform electric-field-induced alteration in the emulsion rheology when the imposed shear flow is weak [30]. However, the dilute emulsion does not show shear thinning or thickening behavior in the weak-flow limit but exhibits normal stress differences [30].

All the reported studies [29,30] have explored the effect of a uniform electric field for the particular case in which the electric field is acting parallel to the direction of the velocity gradient. However, the direction of the uniform electric field relative to the direction of shear flow can significantly affect the drop shape, drop orientation, and flow field [31,32]. Despite the ease with which the direction of the electric field can be controlled, we are unaware of a study that explores the effect of the orientation of the uniform electric field on the emulsion rheology. Motivated by these considerations, in the present study, a small-deformation analytical theory is developed to understand the problem of the emulsion rheology of a dilute suspension of noninteracting drops in the combined presence of shear flow and an arbitrarily oriented (in the plane of shear flow) uniform electric field. Both the surface charge convection and shape deformation effects are incorporated by performing regular perturbation expansion. We emphasize the physical mechanism in which the direction of the electric

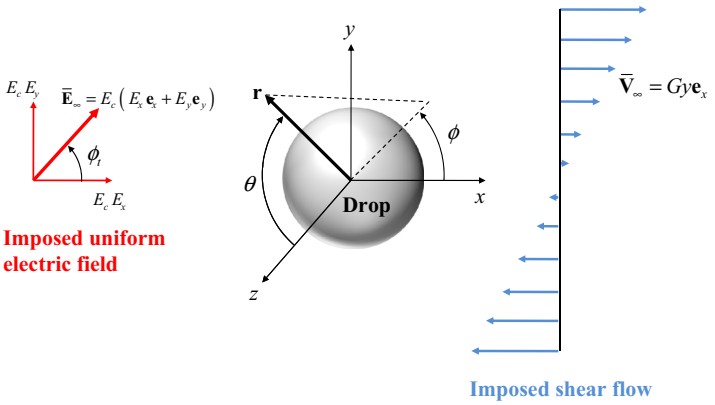

FIG. 1. Schematic representation of the physical setup of a liquid suspended drop subjected to the combined influence of a uniform electric field and background shear flow.

field plays a significant role in manipulating emulsion rheology. We present results for experimentally relevant oil-in-oil emulsions.

II. MATHEMATICAL FORMULATION

A. System description

We consider a physical system comprised of neutrally buoyant, Newtonian, leaky dielectric liquid drops of density ρ, viscosity μ_i, conductivity σ_i, and permittivity ε_i, suspended in another Newtonian, leaky dielectric liquid medium of density ρ, viscosity μ_e, conductivity σ_e, and permittivity ε_e. The drops are immiscible to the suspending medium and the fluid-fluid interface is characterized by a constant surface tension γ. In the absence of external forces, the drops remain spherical in shape with radius a. This equilibrium configuration is disturbed by the combined presence of a uniform electric field $\bar{\mathbf{E}}_\infty$ and background shear flow $\bar{\mathbf{V}}_\infty$ as depicted in Fig. 1. The uniform electric field is of the form $\bar{\mathbf{E}}_\infty = E_c(E_x\mathbf{e}_x + E_y\mathbf{e}_y)$, where E_c is the magnitude of electric field and E_x and E_y represent the relative strength of the electric field in the direction of shear flow and the velocity gradient, respectively. The electric-field vector is oriented at an angle $\phi_t = \tan^{-1}(E_y/E_x)$ with respect to the direction of shear flow (ϕ_t is termed the tilt angle). The background simple shear flow is of the form $\bar{\mathbf{V}}_\infty = Gy\mathbf{e}_x$, where G is the shear rate. The combined presence of $\bar{\mathbf{E}}_\infty$ and $\bar{\mathbf{V}}_\infty$ creates electrical and hydrodynamic stresses across the drop interface, which not only alter the flow field in and around the drops but also deform the drops into nonspherical shape. The altered flow field and shape of the drops affect the shear rheology of a dilute emulsion, the determination of which is the main objective of the present study.

To identify the important dimensionless parameters, we nondimensionalize different quantities by using the following scales [29]: length $\sim a$, velocity $\sim Ga$, electric field $\sim E_c$, viscous stress $\sim\mu_e G$, pressure $\sim\mu_e G$, and electric stress $\sim\varepsilon_e E_c^2$. The present EHD problem can be described by the following dimensionless parameters [29]: viscosity ratio $\lambda = \mu_i/\mu_e$, conductivity ratio $R = \sigma_i/\sigma_e$, permittivity ratio $S = \varepsilon_i/\varepsilon_e$, Reynolds number $\mathrm{Re} = \rho G a^2/\mu_e$ (which is a measure of fluid inertia relative to viscous effect), capillary number $\mathrm{Ca} = \mu_e G a/\gamma$ (which is a measure of viscous stress relative to capillary stress), electric Reynolds number $\mathrm{Re}_E = \varepsilon_e G/\sigma_e$ (which is a measure of charge relaxation time relative to convection time), and Mason number $M = \varepsilon_e E_c^2/\mu_e G$ (which is a measure of electric stress relative to viscous stress). From now on, we represent all quantities in dimensionless form unless stated otherwise. Subscripts i and e will be used to represent quantities inside and outside the drop, respectively. Both Cartesian and spherical coordinates are shown in Fig. 1 with x the direction of shear flow, y the direction of velocity gradient, and z the direction of vorticity.

B. Governing equations and boundary conditions

We assume that both the drop and suspending phases can be described by the leaky dielectric model. The leaky dielectric model takes into account small but finite electric conductivity, which leads to accumulation of electric charges at the fluid-fluid interface, while the bulk remains charge free [33,34]. Thus, the electrostatic problem for leaky dielectric liquids is governed by the Laplace equation for electric potential

$$\nabla^2\psi_i = 0, \quad \nabla^2\psi_e = 0, \tag{1}$$

where ψ represents the electric potential, which is related to the electric field in the form $\mathbf{E} = -\nabla\psi$ (using the irrotationality property of the electric field). The complete description of the electrostatic problem requires further boundary and interfacial conditions. The electric potential outside the drop ψ_e is bounded and satisfies the far-field specified electric potential condition

$$\psi_e = -\mathbf{E}_\infty \cdot \mathbf{r} \quad \text{as } r \to \infty, \tag{2}$$

where $\mathbf{r}$ is the position vector measured from the drop centroid. The electric potential inside the drop ψ_i is bounded. The electric potential at the drop interface is continuous

$$\psi_i = \psi_e \quad \text{at } r = r_s(\theta,\phi), \tag{3}$$

where $r_s(\theta,\phi) = 1 + f(\theta,\phi)$ is the radial position of the deformed drop interface. The function $f(\theta,\phi)$ is an unknown that represents the angular variation of deformed drop shape. The electric potentials satisfy the charging condition at the drop interface [35]

$$\mathbf{n} \cdot (R\nabla\psi_i - \nabla\psi_e) = -\mathrm{Re}_E \nabla_s \cdot (q_s \mathbf{u}_s) \quad \text{at } r = r_s(\theta,\phi), \tag{4}$$

where $q_s = \mathbf{n} \cdot (S\nabla\psi_i - \nabla\psi_e)|_{r=r_s}$ is the surface charge density, $\mathbf{u}_s = \mathbf{u}_i|_{r=r_s}$ is the surface velocity, $\mathbf{n} = \nabla(r - r_s)/|\nabla(r - r_s)|$ is the outward unit normal at the drop interface, and $\nabla_s = [\nabla - \mathbf{n}(\mathbf{n} \cdot \nabla)]$ is the surface divergence operator. Equation (4) shows that the electric Reynolds number Re_E governs the balance between charge convection and Ohmic conduction. The surface charge convection term on the right-hand side of Eq. (4) represents the EHD coupling between electric potential and surface velocity.

We assume that the fluid flow in and around the drop is governed by the viscous forces, while the fluid inertia is negligible (i.e., $\mathrm{Re} = 0$). In the creeping flow limit, the flow field is described by the Stokes and continuity equations in the form

$$\begin{aligned} \nabla p_i &= \lambda\nabla^2\mathbf{u}_i, \quad \nabla \cdot \mathbf{u}_i = 0, \\ \nabla p_e &= \nabla^2\mathbf{u}_e, \quad \nabla \cdot \mathbf{u}_e = 0, \end{aligned} \tag{5}$$

where p and $\mathbf{u}$ represent pressure and velocity fields, respectively. The complete description of the flow problem requires further boundary and interfacial conditions. The pressure and velocity fields outside the drop (p_e and $\mathbf{u}_e$) are bounded. The velocity field outside the drop satisfies the far-field specified shear flow condition

$$\mathbf{u}_e = \mathbf{V}_\infty \quad \text{as } r \to \infty. \tag{6}$$

The velocity and pressure fields inside the drop (p_i and $\mathbf{u}_i$) are bounded. The velocity field at the drop interface is continuous

$$\mathbf{u}_i = \mathbf{u}_e \quad \text{at } r = r_s(\theta,\phi). \tag{7}$$

At steady state, the kinematic condition gives zero normal velocity at the drop interface

$$\mathbf{u}_i \cdot \mathbf{n} = \mathbf{u}_e \cdot \mathbf{n} = 0 \quad \text{at } r = r_s(\theta,\phi). \tag{8}$$

The hydrodynamic and electric stresses are balanced by the capillary stress at the drop interface [35]

$$\left(\boldsymbol{\tau}_e^H + M\boldsymbol{\tau}_e^E\right)\cdot\mathbf{n} - \left(\boldsymbol{\tau}_i^H + M\boldsymbol{\tau}_i^E\right)\cdot\mathbf{n} = \frac{1}{\mathrm{Ca}}(\nabla\cdot\mathbf{n})\mathbf{n} \quad \text{at } r = r_s(\theta,\phi), \tag{9}$$

where $\boldsymbol{\tau}^H$ and $\boldsymbol{\tau}^E$ are hydrodynamic and electric stress tensors of the form

$$\boldsymbol{\tau}_i^H = [-p_i\mathbf{I} + \lambda\{\nabla\mathbf{u}_i + (\nabla\mathbf{u}_i)^T\}], \quad \boldsymbol{\tau}_e^H = [-p_e\mathbf{I} + \{\nabla\mathbf{u}_e + (\nabla\mathbf{u}_e)^T\}] \tag{10}$$

and

$$\boldsymbol{\tau}_i^E = S\left[\mathbf{E}_i(\mathbf{E}_i)^T - \tfrac{1}{2}|\mathbf{E}_i|^2\mathbf{I}\right], \quad \boldsymbol{\tau}_e^E = \left[\mathbf{E}_e(\mathbf{E}_e)^T - \tfrac{1}{2}|\mathbf{E}_e|^2\mathbf{I}\right]. \tag{11}$$

The combination of hydrodynamic and electric stress terms on the left-hand side of Eq. (9) represents the EHD coupling between the flow field and electric stress. Note that Eq. (9) combines both the tangential and normal components of stress balance equations.

C. Description of the electric potential and flow field

The electric potential inside the drop that satisfies the Laplace equation and is bounded for $r \leqslant 1$ can be represented in terms of growing spherical solid harmonics in the form

$$\psi_i = \sum_{n=0}^{\infty} r^n \sum_{m=0}^{n} [a_{n,m}\cos(m\phi) + \hat{a}_{n,m}\sin(m\phi)]P_{n,m}, \tag{12}$$

where $P_{n,m}$ is the associated Legendre polynomial of degree n, order m, and argument $\cos\theta$. Similarly, the electric potential outside the drop that satisfies the Laplace equation and is bounded for $r \geqslant 1$ can be represented in terms of decaying spherical solid harmonics and unperturbed far-field electric potential in the form

$$\psi_e = -\mathbf{E}_\infty\cdot\mathbf{r} + \sum_{n=0}^{\infty} r^{-n-1}\sum_{m=0}^{n}[b_{-n-1,m}\cos(m\phi) + \hat{b}_{-n-1,m}\sin(m\phi)]P_{n,m}. \tag{13}$$

The coefficients $a_{n,m}$, $\hat{a}_{n,m}$, $b_{-n-1,m}$, and $\hat{b}_{-n-1,m}$ are unknown, which we have to determine by using the boundary conditions given in Eqs. (3) and (4).

The velocity and pressure fields inside the drop, which satisfy the Stokes and continuity equations and are bounded for $r \leqslant 1$, can be represented in terms of growing spherical solid harmonics by using Lamb's general solution in the form [36]

$$\mathbf{u}_i = \sum_{n=1}^{\infty}\left[\nabla\times(\mathbf{r}\chi_n) + \nabla\Phi_n + \frac{n+3}{2(n+1)(2n+3)\lambda}r^2\nabla p_n - \frac{n}{(n+1)(2n+3)\lambda}\mathbf{r}p_n\right], \tag{14}$$

$$p_i = \sum_{n=0}^{\infty} p_n, \tag{15}$$

where p_n, Φ_n, and χ_n are the growing spherical solid harmonics of the form

$$p_n = \lambda r^n \sum_{m=0}^{n} [A_{n,m}\cos(m\phi) + \hat{A}_{n,m}\sin(m\phi)]P_{n,m},$$

$$\Phi_n = r^n \sum_{m=0}^{n} [B_{n,m}\cos(m\phi) + \hat{B}_{n,m}\sin(m\phi)]P_{n,m},$$

$$\chi_n = r^n \sum_{m=0}^{n} [C_{n,m}\cos(m\phi) + \hat{C}_{n,m}\sin(m\phi)]P_{n,m}. \tag{16}$$

Similarly, the velocity and pressure fields outside the drop, which satisfy the Stokes and continuity equations and are bounded for $r \geqslant 1$ can be represented in terms of decaying spherical solid harmonics and unperturbed far-field velocity field by using Lamb's general solution in the form [36]

$$\mathbf{u}_e = \mathbf{V}_\infty + \sum_{n=1}^{\infty}\left[\nabla\times(\mathbf{r}\chi_{-n-1}) + \nabla\Phi_{-n-1} - \frac{n-2}{2n(2n-1)}r^2\nabla p_{-n-1} + \frac{n+1}{n(2n-1)}\mathbf{r}p_{-n-1}\right], \tag{17}$$

$$p_e = \sum_{n=0}^{\infty} p_{-n-1}, \tag{18}$$

where p_{-n-1}, χ_{-n-1}, and Φ_{-n-1} are decaying spherical solid harmonics of the form

$$p_{-n-1} = r^{-n-1} \sum_{m=0}^{n} [A_{-n-1,m}\cos(m\phi) + \hat{A}_{-n-1,m}\sin(m\phi)]P_{n,m},$$

$$\Phi_{-n-1} = r^{-n-1} \sum_{m=0}^{n} [B_{-n-1,m}\cos(m\phi) + \hat{B}_{-n-1,m}\sin(m\phi)]P_{n,m},$$

$$\chi_{-n-1} = r^{-n-1} \sum_{m=0}^{n} [C_{-n-1,m}\cos(m\phi) + \hat{C}_{-n-1,m}\sin(m\phi)]P_{n,m}. \tag{19}$$

The coefficients $A_{n,m}$, $\hat{A}_{n,m}$, $B_{n,m}$, $\hat{B}_{n,m}$, $C_{n,m}$, $\hat{C}_{n,m}$, $A_{-n-1,m}$, $\hat{A}_{-n-1,m}$, $B_{-n-1,m}$, $\hat{B}_{-n-1,m}$, $C_{-n-1,m}$, and $\hat{C}_{-n-1,m}$ are unknowns, which we have to determine by using the boundary conditions given in Eqs. (7)–(9).

D. Effective stress of a dilute emulsion of noninteracting drops

The effective shear rheology of an emulsion comprised of a dilute suspension of noninteracting drops is different from that of the shear rheology of the suspending fluid. This is attributed to the disturbance flow generated by the drops. The applied electric field modifies the drop shape, drop orientation, and flow field due to the generation of electrical stresses at the drop interface. The volume average effective emulsion stress $\mathbf{\Sigma}$ for a dilute suspension of force-free drops can be represented as [37–39]

$$\mathbf{\Sigma} = -p\mathbf{I} + 2\mathbf{\Gamma} + \mathbf{\Sigma}^{(d)}, \tag{20}$$

where p is some arbitrary pressure field in the suspending medium (which gives an isotropic contribution to stress), $\mathbf{\Gamma} = [(\nabla\mathbf{V}_\infty) + (\nabla\mathbf{V}_\infty)^T]/2$ is the rate of strain tensor in the suspending medium (which represents the extensional or straining component of imposed shear flow), and $\mathbf{\Sigma}^{(d)}$ is the stresslet tensor (which represents the excess stress generated due to presence of drops). Here $\mathbf{\Sigma}^{(d)}$ gives rise to anisotropy in the emulsion stress. The stresslet tensor for a dilute emulsion (with

ν the volume fraction of drop phase) is given by [38]

$$\mathbf{\Sigma}^{(d)} = \frac{3\nu}{4\pi}\int_{S_d}\left(\frac{1}{2}\left\{\left(\boldsymbol{\tau}_e^H\cdot\mathbf{n}\right)\mathbf{r}+\left[\left(\boldsymbol{\tau}_e^H\cdot\mathbf{n}\right)\mathbf{r}\right]^T-\frac{2}{3}\mathbf{I}\left(\boldsymbol{\tau}_e^H\cdot\mathbf{n}\right)\cdot\mathbf{r}\right\}-\left[\mathbf{u}_e\mathbf{n}+(\mathbf{u}_e\mathbf{n})^T\right]\right)dS_d, \quad (21)$$

where the integration has to be performed over the drop surface S_d. The integral on the right-hand side of Eq. (21) can be obtained as [39,40]

$$\int_{S_d}\left[\frac{1}{2}\left(\left(\boldsymbol{\tau}_e^H\cdot\mathbf{n}\right)\mathbf{r}+\left[\left(\boldsymbol{\tau}_e^H\cdot\mathbf{n}\right)\mathbf{r}\right]^T-\frac{2}{3}\mathbf{I}\left(\boldsymbol{\tau}_e^H\cdot\mathbf{n}\right)\cdot\mathbf{r}\right)-\left[\mathbf{u}_e\mathbf{n}+(\mathbf{u}_e\mathbf{n})^T\right]\right]dS_d$$
$$=\left(-\frac{2\pi}{3}\right)\nabla\nabla(r^5 p_{-3}), \quad (22)$$

where $p_{-3}=r^{-3}\sum_{m=0}^{2}[A_{-3,m}\cos(m\phi)+\hat{A}_{-3,m}\sin(m\phi)]P_{3,m}$ is a decaying solid harmonic.

It is convenient to define three important dynamical quantities to characterize an incompressible homogeneous emulsion. The first one is the effective shear viscosity, which can be expressed in dimensional terms as [41]

$$\mu_{\text{eff}}=\frac{\bar{\Sigma}_{xy}}{G}, \quad (23)$$

where the dimensional stress component $\bar{\Sigma}_{xy}$ can be expressed as $\bar{\Sigma}_{xy}=\mu_e G\Sigma_{xy}$. The effective shear viscosity reflects the viscous nature of the emulsion. The second and third quantities of interest are the first and second normal stress differences, which reflect the elastic nature of the emulsion and the nonisotropy of normal stresses. The first and second normal stress differences can be expressed in dimensional terms as [41]

$$\bar{N}_1=\bar{\Sigma}_{xx}-\bar{\Sigma}_{yy}, \quad \bar{N}_2=\bar{\Sigma}_{yy}-\bar{\Sigma}_{zz}. \quad (24)$$

The dimensionless effective viscosity (normalized by μ_e) and normal stress differences (normalized by $\mu_e G$) can be written as

$$\eta_{\text{eff}}=\frac{\mu_{\text{eff}}}{\mu_e}=\Sigma_{xy}, \quad N_1=\frac{\bar{\Sigma}_{xx}-\bar{\Sigma}_{yy}}{\mu_e G}=\Sigma_{xx}-\Sigma_{yy}, \quad N_2=\frac{\bar{\Sigma}_{yy}-\bar{\Sigma}_{zz}}{\mu_e G}=\Sigma_{yy}-\Sigma_{zz}. \quad (25)$$

Substituting the value of the integral from Eq. (22) into Eq. (21), we obtain the general expression for the effective viscosity and normal stress differences

$$\eta_{\text{eff}}=1-3\nu\hat{A}_{-3,2}, \quad N_1=-6\nu A_{-3,2}, \quad N_2=\frac{3\nu}{2}(2A_{-3,2}+A_{-3,0}). \quad (26)$$

III. ASYMPTOTIC SOLUTION FOR WEAK FLOW AND WEAK CHARGE CONVECTION

The exact solution of the present electrohydrodynamic problem is not possible for arbitrary values of the dimensionless parameters, due to the nonlinearities and coupled nature of the mathematic model. The first source of difficulty is associated with the drop shape, which is not known *a priori*. Determination of the drop shape involves electric and hydrodynamic stresses at the drop interface, while determination of the electric potential and flow field involves the drop shape. Thus, an analytical solution cannot be obtained for arbitrary drop shape. However, an analytical solution can be obtained for small drop deformation in which the drop remains nearly spherical. This can be accomplished by two different ways for two different physical systems [42]: (i) weak flow or a small-capillary-number limit (i.e., Ca $\ll 1$) and (ii) high-viscosity ratio limit (i.e., $\lambda \gg 1$). Vlahovska [29] has performed a small-deformation perturbation analysis for the high-viscosity limit for the particular case in which the applied electric field is oriented in the direction of the velocity gradient (i.e., $\mathbf{E}_\infty=\mathbf{e}_y$). Here we explore the weak-flow limit, which physically signifies that the imposed flow is too weak to deform the drop significantly. In the presence of an electric field, the drop deformation is also influenced by the electric capillary number $\text{Ca}_E=\text{Ca}M$, which signifies the relative strength of electric stress

as compared with capillary stress [35]. Thus, in addition to $\mathrm{Ca} \ll 1$ we also assume $M \sim 1$, so deformation due to electric stress is also small.

The second source of difficulty in the present mathematical model is associated with the surface charge convection, which couples the electric field and flow field. Due to charge convection, determination of the electric field requires the knowledge of surface velocity. Thus, an analytical solution cannot be obtained for arbitrary values of Re_E. However, an analytical solution can be obtained for weak charge convection in which the charge distribution over the drop surface is dominated by the Ohmic conduction. This can be accomplished by considering $\mathrm{Re}_E \ll 1$ [43]. Thus, in the present study we address the weak-flow and weak-charge-convection limits by performing a regular perturbation analysis considering Ca and Re_E as perturbation parameters. Ha and Yang [22] performed experiments on the emulsion of silicone oil drops (with $\mu_i = 0.13$ Pa s, $\sigma_i = 6.2 \times 10^{-12}$ S/m, and $\varepsilon_i = 5.2\varepsilon_0$, where ε_0 is the permittivity of free space) suspended in a castor oil medium (with $\mu_e = 0.85$ Pa s, $\sigma_e = 6.6 \times 10^{-10}$ S/m, and $\varepsilon_e = 2.7\varepsilon_0$). For a physical system of silicone oil drops of radius $a = 100$ μm in the presence of an electric-field strength of $E_c = 4 \times 10^5$ V/m and shear rate of $G = 2.5$ s^{-1}, we obtain $\mathrm{Ca} \sim 0.1$, $\mathrm{Re}_E \sim 0.1$, $M \sim 1$, and $\mathrm{Re} \sim 10^{-3}$. To study this kind of system, we expand the electric potential and velocity field in the asymptotic form [35]

$$\begin{aligned} \psi &= \psi^{(0)} + \mathrm{Re}_E \psi^{(\mathrm{Re}_E)} + \mathrm{Ca}\psi^{(\mathrm{Ca})} + \cdots, \\ \mathbf{u} &= \mathbf{u}^{(0)} + \mathrm{Re}_E \mathbf{u}^{(\mathrm{Re}_E)} + \mathrm{Ca}\mathbf{u}^{(\mathrm{Ca})} + \cdots. \end{aligned} \tag{27}$$

A similar expansion is also employed for all the dependent variables such as surface charge distribution, pressure, and stresses. Note that the superscript (0) is used to represent the leading-order quantity (in the absence of charge convection and shape deformation), (Re_E) is used to represent the first correction due to charge convection, and (Ca) is used to represent the first correction due to shape deformation.

The radial position of the deformed drop is also expanded in the asymptotic form [31,44]

$$r_s = 1 + f(\theta,\phi) = 1 + \mathrm{Ca} f^{(\mathrm{Ca})} + \mathrm{Ca}\,\mathrm{Re}_E f^{(\mathrm{Ca}\,\mathrm{Re}_E)} + \mathrm{Ca}^2 f^{(\mathrm{Ca}^2)} + \cdots, \tag{28}$$

where $f^{(\mathrm{Ca})}$, $f^{(\mathrm{Ca}\,\mathrm{Re}_E)}$, and $f^{(\mathrm{Ca}^2)}$ are the corrections in drop shape at respective orders. Here $f^{(\mathrm{Ca})}$ represents the first correction in drop shape, $f^{(\mathrm{Ca}\,\mathrm{Re}_E)}$ represents the first effect of charge convection on the shape deformation, and $f^{(\mathrm{Ca}^2)}$ represents the $O(\mathrm{Ca}^2)$ correction in drop shape.

Here we obtain solutions for leading-order $O(\mathrm{Re}_E)$ and $O(\mathrm{Ca})$ problems sequentially. The main objective is to determine the effective emulsion stress of a dilute emulsion for $O(\nu)$, $O(\nu\,\mathrm{Re}_E)$, and $O(\nu\,\mathrm{Ca})$. Important to note here is that our analysis is restricted to a dilute emulsion, so $\nu \ll 1$. We are not considering the higher-order corrections in volume fraction [e.g., $O(\nu^2)$, which might be of significance when there are drop-drop EHD interactions for higher volume fractions [45]] by assuming $\mathrm{Ca} > \nu$ and $\mathrm{Re}_E > \nu$. The solution method is straight forward and details can be found in the reported studies [31,32]. Here we outline the important steps for completeness. Note that all the algebraic manipulations are performed using the symbolic package MAPLE. After substituting the asymptotic expansion for different variables, we obtain the governing equations and respective boundary conditions at different orders [31,32]. We use the following steps to obtain different quantifies of interest [35]. (i) At each order, the electrostatic problem becomes linear and decoupled from the flow problem at that order. Thus, we first determine the electric potential and obtain the electric stresses at the drop interface. (ii) Then the flow problem can be solved by using these electric stresses. To do this we use the velocity and tangential stress boundary conditions to obtain the velocity and pressure fields. (iii) The stresslet tensor is calculated to obtain the effective shear viscosity and normal stress differences. (iv) The normal stress balance equation is employed to determine the drop shape.

A. Leading-order solution

The leading-order electric potential distribution is due to the imposed uniform electric field $\mathbf{E}_\infty$. There is no convection of charges and the drop remains spherical, which means that the leading-order electrostatic problem is linear and decoupled from the leading-order flow problem. Thus, we first solve for the electrostatic problem. The electric potential distribution inside and outside the drop at the leading order is obtained as

$$\psi_i^{(0)} = r\left[a_{1,1}^{(0)}\cos\phi + \hat{a}_{1,1}^{(0)}\sin\phi\right]P_{1,1} \tag{29}$$

and

$$\psi_e^{(0)} = -r[E_x P_{1,1}\cos\phi + E_y P_{1,1}\sin\phi] + r^{-2}\left[b_{-2,1}^{(0)}\cos\phi + \hat{b}_{-2,1}^{(0)}\sin\phi\right]P_{1,1}, \tag{30}$$

where the unknown coefficients are obtained as

$$a_{1,1}^{(0)} = -\frac{3E_x}{R+2}, \quad \hat{a}_{1,1}^{(0)} = -\frac{3E_y}{R+2}, \quad b_{-2,1}^{(0)} = E_x\left(\frac{R-1}{R+2}\right), \quad \hat{b}_{-2,1}^{(0)} = E_y\left(\frac{R-1}{R+2}\right). \tag{31}$$

The leading-order surface charge distribution is obtained as

$$q_s^{(0)} = \mathbf{e}_r\cdot\left(R\nabla\psi_i^{(0)} - \nabla\psi_e^{(0)}\right)\big|_{r=1} = \left[c_{1,1}^{(0)}\cos\phi + \hat{c}_{1,1}^{(0)}\sin\phi\right]P_{1,1}, \tag{32}$$

where $c_{1,1}^{(0)}$ and $\hat{c}_{1,1}^{(0)}$ are of the form

$$c_{1,1}^{(0)} = 3\left(\frac{R-S}{R+2}\right)E_x, \quad \hat{c}_{1,1}^{(0)} = 3\left(\frac{R-S}{R+2}\right)E_y. \tag{33}$$

The leading-order flow field is due to the generation of electrical stresses and the imposed shear flow. As the leading-order flow problem is linear in electrical stress and shear flow, we can obtain the total velocity and pressure fields by simply linearly combining the velocity and pressure fields due to imposed uniform electric field and imposed simple shear flow

$$\begin{aligned}\mathbf{u}_i^{(0)} &= \mathbf{u}_i^{E(0)} + \mathbf{u}_i^{S(0)}, \quad p_i^{(0)} = p_i^{E(0)} + p_i^{S(0)},\\ \mathbf{u}_e^{(0)} &= \mathbf{u}_e^{E(0)} + \mathbf{u}_e^{S(0)}, \quad p_e^{(0)} = p_e^{E(0)} + p_e^{S(0)},\end{aligned} \tag{34}$$

where the superscripts E and S are used to represent the contributions from the uniform electric field and shear flow, respectively. The velocity and pressure fields inside the drop due to a uniform electric field and shear flow are obtained as

$$\begin{aligned}\mathbf{u}_i^{E(0)} &= \nabla\Phi_2^{E(0)} + \frac{5}{42\lambda}r^2\nabla p_2^{E(0)} - \frac{2}{21\lambda}\mathbf{r}p_2^{E(0)},\\ \mathbf{u}_i^{S(0)} &= \nabla\times\left(\mathbf{r}\chi_1^{S(0)}\right) + \nabla\Phi_2^{S(0)} + \frac{5}{42\lambda}r^2\nabla p_2^{S(0)} - \frac{2}{21\lambda}\mathbf{r}p_2^{S(0)}\end{aligned} \tag{35}$$

and

$$p_i^{E(0)} = p_2^{E(0)}, \quad p_i^{S(0)} = p_2^{S(0)}, \tag{36}$$

where the expression for the solid harmonics is mentioned in Appendix A. The velocity and pressure fields outside the drop due to a uniform electric field and shear flow are obtained as

$$\mathbf{u}_e^{E(0)} = \nabla\Phi_{-3}^{E(0)} + \tfrac{1}{2}\mathbf{r}p_{-3}^{E(0)}, \quad \mathbf{u}_e^{S(0)} = \nabla\Phi_{-3}^{S(0)} + \tfrac{1}{2}\mathbf{r}p_{-3}^{S(0)} \tag{37}$$

and

$$p_e^{E(0)} = p_{-3}^{E(0)}, \quad p_e^{S(0)} = p_{-3}^{S(0)}, \tag{38}$$

where the expression for the solid harmonics is mentioned in Appendix A.

After obtaining the velocity and pressure fields, we determine the hydrodynamic stress tensor and substitute it in Eq. (20) to obtain the effective emulsion stress. The leading-order effective viscosity is obtained as

$$\eta_{\text{eff}}^{(0)} = 1 - 3\nu \hat{A}_{-3,2}^{(0)}. \tag{39}$$

Substituting the expression for $\hat{A}_{-3,2}^{(0)}$, we obtain $\eta_{\text{eff}}^{(0)}$ as

$$\eta_{\text{eff}}^{(0)} = \underbrace{\left[1 + \nu\left(\frac{5\lambda + 2}{2\lambda + 2}\right)\right]}_{\eta_{\text{eff},T}^{(0)}} + \underbrace{\nu\left[\frac{27}{5}\frac{E_x E_y M(S-R)}{(R+2)^2(\lambda+1)}\right]}_{\eta_{\text{eff},E}^{(0)}}. \tag{40}$$

The term $\eta_{\text{eff},T}^{(0)}$ represents the emulsion viscosity in the absence of an electric field, which was first obtained by Taylor [8]. The term $\eta_{\text{eff},E}^{(0)}$ is an extra contribution due to the applied electric field.

The leading-order normal stress differences are obtained as

$$N_1^{(0)} = -6\nu A_{-3,2}^{(0)}, \quad N_2^{(0)} = \frac{3\nu}{2}\left(2A_{-3,2}^{(0)} + A_{-3,0}^{(0)}\right). \tag{41}$$

Substituting the expressions of $A_{-3,0}^{(0)}$ and $A_{-3,2}^{(0)}$, we obtain $N_1^{(0)}$ and $N_2^{(0)}$ as

$$\begin{aligned} N_1^{(0)} &= \frac{27}{5}\frac{\nu(E_x^2 - E_y^2)M(S-R)}{(R+2)^2(\lambda+1)}, \\ N_2^{(0)} &= \frac{27}{5}\frac{\nu E_y^2 M(S-R)}{(R+2)^2(\lambda+1)}. \end{aligned} \tag{42}$$

B. The $O(\text{Re}_E)$ solution

The $O(\text{Re}_E)$ electric potential distribution is due to the fluid flow-induced redistribution of charges at the drop surface. The $O(\text{Re}_E)$ charging condition can be written as

$$\mathbf{e}_r \cdot \left(R\nabla\psi_i^{(\text{Re}_E)} - \nabla\psi_e^{(\text{Re}_E)}\right)\big|_{r=1} = -\nabla_s \cdot \left(q_s^{(0)}\mathbf{u}_s^{(0)}\right)\big|_{r=1}. \tag{43}$$

The right-hand side of Eq. (43) can be expressed in terms of surface harmonics as

$$\begin{aligned} -\nabla_s \cdot \left(q_s^{(0)}\mathbf{u}_s^{(0)}\right)\big|_{r=1} = \{&(Z_{1,1}\cos\phi + \hat{Z}_{1,1}\sin\phi)P_{1,1} + (Z_{3,1}\cos\phi + \hat{Z}_{3,1}\sin\phi)P_{3,1} \\ &+ [Z_{3,3}\cos(3\phi) + \hat{Z}_{3,3}\sin(3\phi)]P_{3,3}\}, \end{aligned} \tag{44}$$

where the coefficients $Z_{n,m}$ and $\hat{Z}_{n,m}$ are obtained in terms of the coefficients present in $\mathbf{u}_i^{E(0)}$, $\mathbf{u}_i^{S(0)}$, and $q_s^{(0)}$ (refer to Appendix B for detailed expressions). It is apparent from Eq. (44) that the $O(\text{Re}_E)$ electric potential distributions inside and outside the drop are of the form

$$\begin{aligned} \psi_i^{(\text{Re}_E)} = \big\{&r\left(a_{1,1}^{(\text{Re}_E)}\cos\phi + \hat{a}_{1,1}^{(\text{Re}_E)}\sin\phi\right)P_{1,1} + r^3\left(a_{3,1}^{(\text{Re}_E)}\cos\phi + \hat{a}_{3,1}^{(\text{Re}_E)}\sin\phi\right)P_{3,1} \\ &+ r^3\left[a_{3,3}^{(\text{Re}_E)}\cos(3\phi) + \hat{a}_{3,3}^{(\text{Re}_E)}\sin(3\phi)\right]P_{3,3}\big\} \end{aligned} \tag{45}$$

and

$$\begin{aligned} \psi_e^{(\text{Re}_E)} = \big[&r^{-2}\left(b_{-2,1}^{(\text{Re}_E)}\cos\phi + \hat{b}_{-2,1}^{(\text{Re}_E)}\sin\phi\right)P_{1,1} + r^{-4}\left(b_{-4,1}^{(\text{Re}_E)}\cos\phi + \hat{b}_{-4,1}^{(\text{Re}_E)}\sin\phi\right)P_{3,1} \\ &+ r^{-4}\left(b_{-4,3}^{(\text{Re}_E)}\cos\phi + \hat{b}_{-4,3}^{(\text{Re}_E)}\sin\phi\right)P_{3,3}\big], \end{aligned} \tag{46}$$

where the unknown coefficients are obtained as

$$a_{n,m}^{(\mathrm{Re}_E)} = b_{-n-1,m}^{(\mathrm{Re}_E)} = \frac{Z_{n,m}}{n(R+1)+1}, \quad \hat{a}_{n,m}^{(\mathrm{Re}_E)} = \hat{b}_{-n-1,m}^{(\mathrm{Re}_E)} = \frac{\hat{Z}_{n,m}}{n(R+1)+1}. \tag{47}$$

The $O(\mathrm{Re}_E)$ surface charge distribution is obtained as

$$q_s^{(Re_E)} = \mathbf{e}_r \cdot \left(S\nabla\psi_i^{(Re_E)} - \nabla\psi_e^{(Re_E)}\right) = \left[c_{1,1}^{(Re_E)}\cos\phi + \hat{c}_{1,1}^{(Re_E)}\sin\phi\right]P_{1,1} + \left[c_{3,1}^{(Re_E)}\cos\phi + \hat{c}_{3,1}^{(Re_E)}\sin\phi\right]P_{3,1} + \left[c_{3,3}^{(Re_E)}\cos(3\phi) + \hat{c}_{3,3}^{(Re_E)}\sin(3\phi)\right]P_{3,3}, \tag{48}$$

where $c_{n,m}^{(Re_E)} = Z_{n,m}[n(S+1)+1]/[n(R+1)+1]$ and $\hat{c}_{n,m}^{(Re_E)} = \hat{Z}_{n,m}[n(S+1)+1]/[n(R+1)+1]$.

The $O(\mathrm{Re}_E)$ flow field is due to the $O(\mathrm{Re}_E)$ electrical stresses. The velocity and pressure fields inside the drop are obtained as

$$\mathbf{u}_i^{(\mathrm{Re}_E)} = \left[\nabla\times\left\{\mathbf{r}\left(\chi_1^{(\mathrm{Re}_E)} + \chi_3^{(\mathrm{Re}_E)}\right)\right\} + \nabla\left(\Phi_2^{(\mathrm{Re}_E)} + \Phi_4^{(\mathrm{Re}_E)}\right) + \frac{r^2}{\lambda}\left(\frac{5}{42}\nabla p_2^{(\mathrm{Re}_E)} + \frac{7}{110}\nabla p_4^{(\mathrm{Re}_E)}\right) - \frac{\mathbf{r}}{\lambda}\left(\frac{2}{21}p_2^{(\mathrm{Re}_E)} + \frac{4}{55}p_4^{(\mathrm{Re}_E)}\right)\right] \tag{49}$$

and

$$p_i^{(\mathrm{Re}_E)} = p_2^{(\mathrm{Re}_E)} + p_4^{(\mathrm{Re}_E)}, \tag{50}$$

where the expression for the solid harmonics are mentioned in Appendix B. The velocity and pressure fields outside the drop are obtained as

$$\mathbf{u}_e^{(\mathrm{Re}_E)} = \left[\nabla\times\left\{\mathbf{r}\left(\chi_{-2}^{(\mathrm{Re}_E)} + \chi_{-4}^{(\mathrm{Re}_E)}\right)\right\} + \nabla\left(\Phi_{-3}^{(\mathrm{Re}_E)} + \Phi_{-5}^{(\mathrm{Re}_E)}\right) - \frac{r^2}{28}\nabla p_{-5}^{(\mathrm{Re}_E)} + \mathbf{r}\left(\frac{1}{2}p_{-3}^{(\mathrm{Re}_E)} + \frac{1}{28}p_{-5}^{(\mathrm{Re}_E)}\right)\right] \tag{51}$$

and

$$p_e^{(\mathrm{Re}_E)} = p_{-3}^{(\mathrm{Re}_E)} + p_{-5}^{(\mathrm{Re}_E)}, \tag{52}$$

where the expression for the solid harmonics are mentioned in Appendix B.

After obtaining the velocity and pressure fields, we determine the hydrodynamic stress tensor and substitute it in Eq. (20) to obtain the effective emulsion stress. The $O(\mathrm{Re}_E)$ effective viscosity is obtained as

$$\eta_{\mathrm{eff}}^{(\mathrm{Re}_E)} = -3\nu\hat{A}_{-3,2}^{(\mathrm{Re}_E)}. \tag{53}$$

Substituting the expression of $\hat{A}_{-3,2}^{(\mathrm{Re}_E)}$, we obtain $\eta_{\mathrm{eff}}^{(\mathrm{Re}_E)}$ as

$$\eta_{\mathrm{eff}}^{(\mathrm{Re}_E)} = \frac{\nu M\left[\frac{9}{10}\frac{R-2S-2}{R+2}(E_y Z_{1,1} + E_x\hat{Z}_{1,1}) - \frac{4R+4-S}{3R+4}\left[\frac{9}{35}(E_y Z_{3,1} + E_x\hat{Z}_{3,1}) + \frac{54}{7}(E_y Z_{3,3} - E_x\hat{Z}_{3,3})\right]\right]}{(R+2)(\lambda+1)}. \tag{54}$$

The $O(\mathrm{Re}_E)$ normal stress differences are obtained as

$$N_1^{(\mathrm{Re}_E)} = -6\nu A_{-3,2}^{(\mathrm{Re}_E)}, \quad N_2^{(\mathrm{Re}_E)} = \frac{3\nu}{2}\left(2A_{-3,2}^{(\mathrm{Re}_E)} + A_{-3,0}^{(\mathrm{Re}_E)}\right). \tag{55}$$

Substituting the expressions of $A_{-3,0}^{(\mathrm{Re}_E)}$ and $A_{-3,2}^{(\mathrm{Re}_E)}$, we obtain $N_1^{(\mathrm{Re}_E)}$ and $N_2^{(\mathrm{Re}_E)}$ as

$$N_1^{(\mathrm{Re}_E)} = \frac{\nu M\left[\frac{9}{5}\frac{R-2S-2}{R+2}(E_x Z_{1,1} - E_y \hat{Z}_{1,1}) - \frac{4R+4-S}{3R+4}\left[\frac{18}{35}(E_x Z_{3,1} - E_y \hat{Z}_{3,1}) - \frac{108}{7}(E_x Z_{3,3} + E_y \hat{Z}_{3,3})\right]\right]}{(R+2)(\lambda+1)} \tag{56}$$

and

$$N_2^{(\mathrm{Re}_E)} = \frac{\nu M\left[\frac{9}{5}\frac{R-2S-2}{R+2}E_y \hat{Z}_{1,1} - \left(\frac{4R+4-S}{3R+4}\right)\left[\frac{9}{7}E_x Z_{3,1} + \frac{9}{5}E_y \hat{Z}_{3,1} + \frac{54}{7}(E_x Z_{3,3} + E_y \hat{Z}_{3,3})\right]\right]}{(R+2)(\lambda+1)}. \tag{57}$$

C. The O(Ca) solution

First we determine the $O(\mathrm{Ca})$ correction in drop shape, which can be obtained by using the leading-order solution. The deformed drop shape correct up to the $O(\mathrm{Ca})$ term can be expressed as

$$r_s(\theta,\phi) = 1 + \mathrm{Ca}\, f^{(\mathrm{Ca})}, \tag{58}$$

where $f^{(\mathrm{Ca})}$ is obtained as

$$f^{(\mathrm{Ca})} = L_{2,0}^{(\mathrm{Ca})} P_{2,0} + L_{2,2}^{(\mathrm{Ca})} \cos(2\phi) P_{2,2} + \hat{L}_{2,2}^{(\mathrm{Ca})} \sin(2\phi) P_{2,2}. \tag{59}$$

Different coefficients $L_{2,0}^{(\mathrm{Ca})}$, $L_{2,2}^{(\mathrm{Ca})}$, and $\hat{L}_{2,0}^{(\mathrm{Ca})}$ are obtained in the form

$$L_{2,0}^{(Ca)} = -\frac{3}{8}\frac{\left(E_x^2 + E_y^2\right)M\Omega_T}{(R+2)^2}, \quad L_{2,2}^{(Ca)} = \frac{3}{16}\frac{\left(E_x^2 - E_y^2\right)M\Omega_T}{(R+2)^2}, \quad \hat{L}_{2,2}^{(Ca)} = \frac{5}{12}D_T + \frac{3}{8}\frac{E_x E_y M\Omega_T}{(R+2)^2}, \tag{60}$$

where $\Omega_T = R^2 + 1 - 2S + 3(R-S)(3\lambda+2)/5(\lambda+1)$ is the Taylor discrimination function and $D_T = (19\lambda+16)/(20\lambda+20)$ is the Taylor deformation parameter.

The $O(\mathrm{Ca})$ electric potential is due to the deformed drop shape. The $O(\mathrm{Ca})$ electric potential distributions inside and outside the drop are of the form

$$\psi_i^{(Ca)} = r\left[a_{1,1}^{(Ca)} \cos\phi + \hat{a}_{1,1}^{(Ca)} \sin\phi\right] P_{1,1} \tag{61}$$

and

$$\begin{aligned}\psi_e^{(Ca)} = {} & r^{-2}\left[b_{-2,1}^{(Ca)} \cos\phi + \hat{b}_{-2,1}^{(Ca)} \sin\phi\right] P_{1,1} \\ & + r^{-4}\left\{\left(b_{-4,1}^{(Ca)} \cos\phi + \hat{b}_{-4,1}^{(Ca)} \sin\phi\right) P_{3,1} + \left[b_{-4,3}^{(Ca)} \cos(3\phi) + \hat{b}_{-4,3}^{(Ca)} \sin(3\phi)\right] P_{3,3}\right\},\end{aligned} \tag{62}$$

where the unknown coefficients are given in Appendix C. Importantly, the unknown coefficients $a_{n,m}^{(Ca)}$, $\hat{a}_{n,m}^{(Ca)}$, $b_{n,n}^{(Ca)}$, and $b_{-n-1,n}^{(Ca)}$ are linear in $L_{2,0}^{(Ca)}$, $L_{2,2}^{(Ca)}$, and $\hat{L}_{2,2}^{(Ca)}$.

The $O(\mathrm{Ca})$ surface charge distribution can be obtained as

$$\begin{aligned}q_s^{(Ca)} = {} & \left[S\left\{\frac{\partial \psi_i^{(Ca)}}{\partial r} + f^{(Ca)}\frac{\partial^2 \psi_i^{(0)}}{\partial r^2} - \frac{\partial f^{(Ca)}}{\partial \theta}\frac{\partial \psi_i^{(0)}}{\partial \theta} - \frac{1}{\sin^2\theta}\frac{\partial f^{(Ca)}}{\partial \phi}\frac{\partial \psi_i^{(0)}}{\partial \phi}\right\}\right|_{r=1} \\ & - \left\{\frac{\partial \psi_e^{(Ca)}}{\partial r} + f^{(Ca)}\frac{\partial^2 \psi_e^{(0)}}{\partial r^2} - \frac{\partial f^{(Ca)}}{\partial \theta}\frac{\partial \psi_e^{(0)}}{\partial \theta} - \frac{1}{\sin^2\theta}\frac{\partial f^{(Ca)}}{\partial \phi}\frac{\partial \psi_e^{(0)}}{\partial \phi}\right\}\Bigg|_{r=1}\Bigg].\end{aligned} \tag{63}$$

The $O(\mathrm{Ca})$ flow field is due to the deformed drop shape. The velocity and pressure fields inside and outside the drop are obtained as

$$\mathbf{u}_i^{(Ca)} = \sum_{n=1}^{4}\left[\nabla\times\left(\mathbf{r}\chi_n^{(Ca)}\right) + \nabla\Phi_n^{(Ca)} + \frac{n+3}{2(n+1)(2n+3)\lambda}r^2\nabla p_n^{(Ca)} - \frac{n}{(n+1)(2n+3)\lambda}\mathbf{r}p_n^{(Ca)}\right], \tag{64}$$

$$p_i^{(Ca)} = \sum_{n=1}^{4} p_n^{(Ca)}, \tag{65}$$

$$\mathbf{u}_e^{(Ca)} = \sum_{n=1}^{4}\left[\nabla\times\left(\mathbf{r}\chi_{-n-1}^{(Ca)}\right) + \nabla\Phi_{-n-1}^{(Ca)} - \frac{n-2}{2n(2n-1)}r^2\nabla p_{-n-1}^{(Ca)} + \frac{n+1}{n(2n-1)}\mathbf{r}p_{-n-1}^{(Ca)}\right], \tag{66}$$

and

$$p_e^{(Ca)} = \sum_{n=1}^{4} p_{-n-1}^{(Ca)}, \tag{67}$$

where the expression for the solid harmonics are too lengthy to be presented here. Importantly, the solid harmonics are linear in $L_{2,0}^{(Ca)}$, $L_{2,2}^{(Ca)}$, and $\hat{L}_{2,2}^{(Ca)}$.

After obtaining the velocity and pressure fields, we determine the hydrodynamic stress tensor and substitute it in Eq. (20) to obtain the effective emulsion stress. The $O(\mathrm{Ca})$ effective viscosity is obtained as

$$\eta_{\mathrm{eff}}^{(Ca)} = -3\nu\hat{A}_{-3,2}^{(Ca)}. \tag{68}$$

Substituting the expression of $\hat{A}_{-3,2}^{(Ca)}$, we obtain $\eta_{\mathrm{eff}}^{(Ca)}$ as

$$\begin{aligned}\eta_{\mathrm{eff}}^{(Ca)} = \nu\Bigg[&L_{2,0}^{(Ca)}\left\{-\frac{3}{70}\frac{4+25\lambda^2+41\lambda}{(\lambda+1)^2} + \frac{162}{175}\frac{ME_xE_y(-9\lambda+8R-5+6R\lambda)(R-S)}{(\lambda+1)^2(R+2)^3}\right\}\\ &+ L_{2,2}^{(Ca)}\left\{-\frac{3}{5}\frac{16+19\lambda}{\lambda+1}\right\}\\ &+ \hat{L}_{2,2}^{(Ca)}\left\{-\frac{162}{175}\frac{M\left(E_x^2+E_y^2\right)(20R\lambda+22R-23\lambda-19)(R-S)}{(\lambda+1)^2(R+2)^3}\right\}\Bigg].\end{aligned} \tag{69}$$

The $O(\mathrm{Ca})$ normal stress differences are obtained as

$$N_1^{(Ca)} = -6\nu A_{-3,2}^{(Ca)}, \quad N_2^{(Ca)} = \frac{3\nu}{2}\left(2A_{-3,2}^{(Ca)} + A_{-3,0}^{(Ca)}\right). \tag{70}$$

Substituting the expressions of $A_{-3,0}^{(Ca)}$ and $A_{-3,2}^{(Ca)}$, we obtain $N_1^{(Ca)}$ and $N_2^{(Ca)}$ as

$$\begin{aligned}N_1^{(Ca)} = \nu\Bigg[&L_{2,0}^{(Ca)}\left\{\frac{162}{175}\frac{M\left(E_x^2-E_y^2\right)(-9\lambda+8R+6R\lambda-5)(R-S)}{(\lambda+1)^2(R+2)^3}\right\}\\ &+ L_{2,2}^{(Ca)}\left\{-\frac{324}{175}\frac{M\left(E_x^2+E_y^2\right)(-19+20R\lambda-23\lambda+22R)(R-S)}{(\lambda+1)^2(R+2)^3}\right\}\\ &+ \hat{L}_{2,2}^{(Ca)}\left(\frac{6}{5}\frac{19\lambda+16}{\lambda+1}\right)\Bigg]\end{aligned} \tag{71}$$

and

$$N_2^{(Ca)} = \nu\Bigg[L_{2,0}^{(Ca)}\left\{\frac{162}{25}\frac{(R-S)M}{(R+2)^2(\lambda+1)}\left(\frac{E_x^2(\lambda-1)}{7(\lambda+1)}+\frac{E_y^2(R-1)}{R+2}\right)\right\} + L_{2,2}^{(Ca)}\left\{\frac{324}{175}\frac{(R-S)M}{(R+2)^2(\lambda+1)^2}\left(E_x^2(\lambda-1)+E_y^2\frac{-17+19R\lambda+23R-25\lambda}{R+2}\right)\right\} + \hat{L}_{2,2}^{(Ca)}\left\{E_xE_y\left(-\frac{972}{175}\frac{M(-9\lambda+8R-5+6R\lambda)(R-S)}{(\lambda+1)^2(R+2)^3}\right)-\frac{6}{35}\frac{50+29\lambda^2+61\lambda}{(\lambda+1)^2}\right\}\Bigg]. \tag{72}$$

Note that $\eta_{\text{eff}}^{(Ca)}$, $N_1^{(Ca)}$, and $N_2^{(Ca)}$ are linear in $L_{2,0}^{(Ca)}$, $L_{2,2}^{(Ca)}$, and $\hat{L}_{2,2}^{(Ca)}$.

IV. RESULTS AND DISCUSSION

A. Emulsion rheology in the absence of charge convection and shape deformation

When the charge convection and shape deformation effects are negligible, the effective shear viscosity is $\eta_{\text{eff}}^{(0)}$ [refer to Eq. (40)]. A closer look into the expression of $\eta_{\text{eff}}^{(0)}$ reveals that at leading order the effects of imposed shear flow and imposed electric field are decoupled. Here $\eta_{\text{eff},T}^{(0)}$ is a positive quantity, which suggests that the effective viscosity in the absence of an electric field is always greater than the viscosity of the suspending medium (i.e., $\eta_{\text{eff},T}^{(0)} > 1$) with a maximum value in the limit $\lambda \to \infty$. The limit $\lambda \to \infty$ represents the Einstein viscosity limit [38]. The Einstein viscosity limit represents the effective viscosity of a dilute suspension of rigid spheres, which is given by $\eta_{\text{eff}}^{(0)} = 1 + 5\nu/2$. It is important to note that $\eta_{\text{eff},T}^{(0)}$ is independent of shear rate. Thus, a dilute emulsion of drops shows Newtonian behavior in the absence of an electric field. Interestingly, $\eta_{\text{eff},E}^{(0)}$ depends on the shear rate (recall the definition of the Mason number $M = \varepsilon_e E_c^2/\mu_e G$). Thus, the presence of an electric field yields non-Newtonian rheology even in the absence of charge convection and shape deformation. However, the mere presence of an electric field is not sufficient to produce a nonzero contribution of $\eta_{\text{eff},E}^{(0)}$. A closer look into the expression of $\eta_{\text{eff},E}^{(0)}$ reveals that electric field has no contribution to $\eta_{\text{eff}}^{(0)}$ (i.e., $\eta_{\text{eff},E}^{(0)} = 0$) in any of the following conditions: (i) $R = S$, which is tantamount to perfectly dielectric drops suspended in a perfectly dielectric medium; (ii) $R \to \infty$, which means that the dispersed drops are perfectly conducting and the suspending medium is perfectly (or leaky) dielectric; (iii) $\lambda \to \infty$, which means the suspension of rigid spheres; and (iv) $E_xE_y = 0$, which means an electric field in the direction of shear flow (i.e., $\mathbf{E}_\infty = \mathbf{e}_x$) or an electric field in the direction of the velocity gradient (i.e., $\mathbf{E}_\infty = \mathbf{e}_y$). The first three conditions (i.e., $R = S$, $R \to \infty$, and $\lambda \to \infty$) are associated with vanishing EHD flow, while the fourth condition is associated with an EHD flow for which the straining axis is aligned with the direction of shear flow or velocity gradient. Thus, the electric field alters the effective viscosity only when the straining axis of EHD flow is oriented in such a way that $E_xE_y \neq 0$ (which is equivalent to a tilt angle ϕ_t which satisfies $0 < \phi_t < \pi/2$ or $\pi/2 < \phi_t < \pi$) and the drops and suspending medium are leaky dielectric fluids with $R \neq S$. In a reported study, Vlahovska [29] has shown that the electric field does not affect the leading-order effective viscosity when the electric field acts in the velocity gradient direction (i.e., $\mathbf{E}_\infty = \mathbf{e}_y$). We also recover the same behavior.

The physical reason for this altered effective viscosity can be understood by looking into the flow structure around the drop. Imposed shear flow has two components [refer to Fig. 2(a)]: pure straining flow and pure rotational flow. The axis of the straining flow is oriented at an angle $\pi/4$ with the direction of shear flow. The presence of a drop resists this straining component of imposed shear flow, while the rotational component has no effect at leading order [46]. The perturbed flow leads to enhancement of viscous dissipation and thereby increases the effective viscosity. On the other hand,

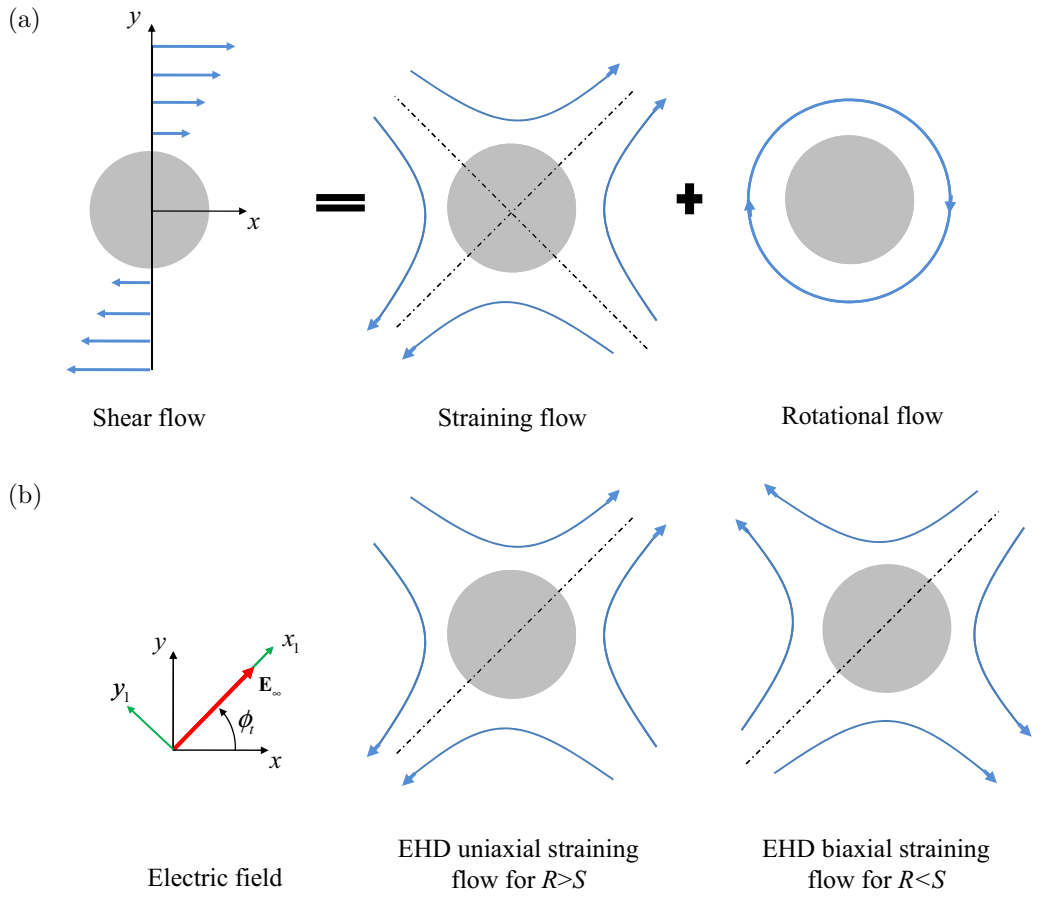

FIG. 2. (a) Schematic representation of the hydrodynamic flow around the drop due to imposed shear flow. (b) Schematic representation of the electrohydrodynamic flow around the drop due to imposed electric field.

the EHD flow generated due to an imbalance of tangential electric stress can be of two types [refer to Fig. 2(b)], uniaxial straining flow and biaxial straining flow, depending on the polarization of the drop [47]. When $R > S$ the drop dipole moment, generated due to the surface charge distribution, aligns with the applied electric field, which leads to generation of uniaxial straining flow. The completely reverse happens (the drop dipole moment orients opposite to the applied electric field, which leads to generation of biaxial straining flow) when $R < S$. The axis of EHD straining flow is always oriented in the direction of applied electric field (i.e., at an angle ϕ_t with the shear flow direction). In the combined presence of shear flow and a uniform electric field, we identify the following three representative situations: (i) an electric field acting in the direction of the velocity gradient (i.e., $\phi_t = \pi/2$), (ii) an electric field acting in the direction of shear flow (i.e., $\phi_t = 0$), and (iii) an electric field acting at an angle $\phi_t = \pi/4$.

If we consider a Cartesian coordinate system in which one axis is along the direction of the applied electric field (x_1) and the other two are orthogonal to the applied electric field (y_1 and z_1), the EHD flow is always axisymmetric in the x_1 direction. This axisymmetric flow gives rise to nonzero diagonal components of the stresslet tensor ($\Sigma^{(d)}_{x_1x_1}$, $\Sigma^{(d)}_{y_1y_1}$, and $\Sigma^{(d)}_{z_1z_1}$); the off-diagonal components ($\Sigma^{(d)}_{x_1y_1}$, $\Sigma^{(d)}_{y_1z_1}$, and $\Sigma^{(d)}_{z_1x_1}$) vanish. This leads to generation of first and second normal stress differences, which are denoted by $\Sigma_{x_1x_1} - \Sigma_{y_1y_1}$ and $\Sigma_{y_1y_1} - \Sigma_{z_1z_1}$. For $\phi_t = \pi/2$ the coordinate system (x_1, y_1, z_1) coincides with $(y, -x, z)$, while for $\phi_t = 0$ the coordinate system (x_1, y_1, z_1) coincides with (x, y, z).

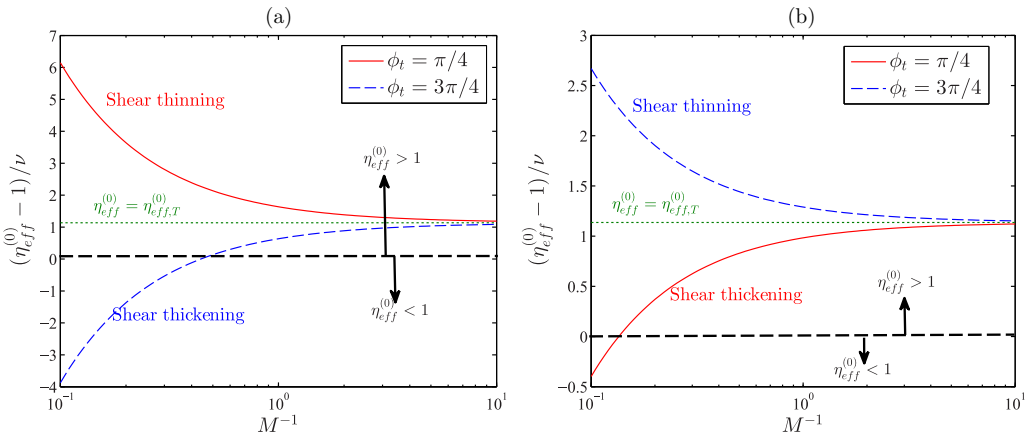

FIG. 3. Variation of normalized effective shear viscosity with normalized shear rate for (a) $R = 0.1$ and (b) $R = 10$. The other parameters are taken as $S = 1$ and $\lambda = 0.1$.

In both these cases, the normal stress differences in the coordinate system (x_1, y_1, z_1) give rise to only normal stress differences in the coordinate system (x, y, z). However, for $\phi_t = \pi/4$ the normal stress differences in the coordinate system (x_1, y_1, z_1) give rise to both effective viscosity (i.e., nonzero off-diagonal components) and normal stress differences in the coordinate system (x, y, z). Thus, the directionality of the applied electric field gives rise to $\eta^{(0)}_{\text{eff},E}$. For $\phi_t = \pi/4$ the EHD flow augments the straining component of imposed shear flow when the EHD flow is uniaxial type (i.e., for $R > S$), while the EHD flow retards the straining component of imposed shear flow when the EHD flow is biaxial type (i.e., for $R < S$). This augmentation (or retardation) of the straining component of imposed shear flow by EHD straining flow leads to a decrease (or increase) in effective viscosity.

To investigate the shear rate dependence of $\eta^{(0)}_{\text{eff}}$, we plot the variation of normalized effective viscosity $(\eta^{(0)}_{\text{eff}} - 1)/\nu$ with the normalized shear rate (which is equivalent to M^{-1} for fixed electric-field strength) in Fig. 3(a) for $(R, S) = (0.1, 1)$ and in Fig. 3(b) for $(R, S) = (10, 1)$. The choice of these property ratios is based on the fact that $(R, S) = (0.1, 1)$ resembles the physical situation of silicone oil drops suspended in castor oil, while $(R, S) = (10, 1)$ resembles the physical situation of castor oil drops suspended in silicone oil [22]. To explicitly show the influence of the electric field, we plot results for $\phi_t = \pi/4$ and $\phi_t = 3\pi/4$. We also plot a $\eta^{(0)}_{\text{eff}} = \eta^{(0)}_{\text{eff},T}$ line, which represents the vanishing effect of the electric field on the effective viscosity. Figure 3(a) shows that for $\phi_t = \pi/4$ the effective viscosity not only is larger than the viscosity of suspending medium (i.e., $\eta^{(0)}_{\text{eff}} > 1$), but also is larger than the effective viscosity when the electric field is absent (i.e., $\eta^{(0)}_{\text{eff}} > \eta^{(0)}_{\text{eff},T}$). This enhancement in viscosity is also evident from Eq. (40), which shows that $\eta^{(0)}_{\text{eff},E}$ is positive for $E_x E_y > 0$ and $R < S$. With an increase in normalized shear rate, the effective viscosity decreases, which means that the emulsion shows shear thinning behavior for $\phi_t = \pi/4$. The completely reverse behavior is depicted in Fig. 3(a) for $\phi_t = 3\pi/4$, which shows shear thickening (an increase in viscosity with an increase in shear rate). We define a critical Mason number (associated with a critical value of the shear rate) for which $(\eta^{(0)}_{\text{eff}} - 1)/\nu = 0$ or $\eta^{(0)}_{\text{eff}} = 1$. The critical Mason number is obtained as

$$\eta^{(0)}_{\text{eff}}(M_{cr}) = 1 \Rightarrow \; M_{cr} = \frac{5}{54}\frac{(R+2)^2(5\lambda+2)}{E_x E_y (R-S)}. \tag{73}$$

For $M < M_{cr}$ the effective viscosity is larger than the viscosity of the suspending medium (i.e., $\eta^{(0)}_{\text{eff}} > 1$), while for $M > M_{cr}$ the effective viscosity is smaller than the viscosity of the suspending medium (i.e., $\eta^{(0)}_{\text{eff}} < 1$). In the latter regime, we obtain negative values of $(\eta^{(0)}_{\text{eff}} - 1)/\nu$, which are associated with a decrease in emulsion viscosity below the viscosity of the suspending medium.

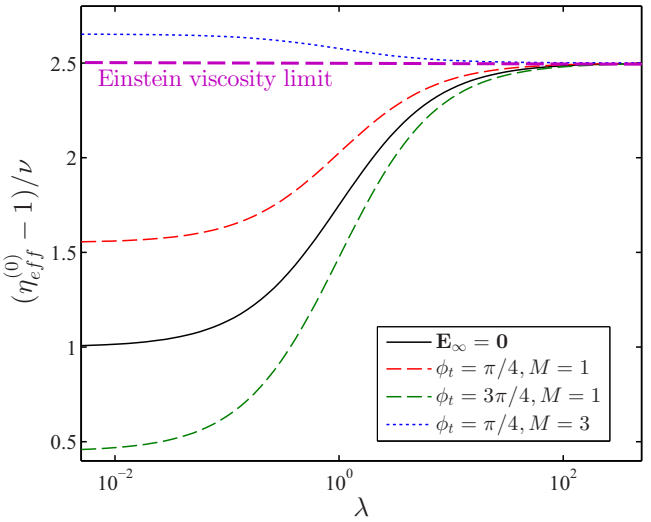

FIG. 4. Variation of normalized effective shear viscosity with viscosity ratio for $R = 0.1$ and $S = 1$.

Thus, a tilted electric field not only induces shear thinning or thickening behavior but also can decrease the emulsion velocity below the viscosity of suspending medium. For higher values of normalized shear rate, the electric field has a negligible effect and both curves (for $\phi_t = \pi/4$ and $\phi_t = 3\pi/4$) approach the same limit (i.e., $\eta^{(0)}_{\text{eff}} \to \eta^{(0)}_{\text{eff},T}$). Figure 3(b) shows that for $\phi_t = \pi/4$ the emulsion shows shear thickening behavior. Importantly, the effective viscosity decreases below the viscosity of the suspending medium for $M > M_{cr}$. However, the emulsion shows shear thinning behavior for all values of the shear rate when $\phi_t = 3\pi/4$. This distinctive behavior of the emulsion of castor oil drops in silicone oil as compared with the emulsion of silicone oil drops in castor oil is due to the fact that $R/S < 1$ for Fig. 3(a), while $R/S > 1$ for Fig. 3(b). Thus, the direction of EHD flow is completely reverse for the two cases under consideration.

To investigate the effect of the tilt angle, we substitute $E_x = \sin\phi_t$ and $E_y = \cos\phi_t$ and obtain that the dependence of $\eta^{(0)}_{\text{eff}}$ on the tilt angle is $\sin(2\phi_t)$. For $(R,S) = (0.1,1)$, the presence of a tilted electric field increases the emulsion viscosity when $0 < \phi_t < \pi/2$ and decreases the emulsion viscosity when $\pi/2 < \phi_t < \pi$. The exactly opposite behavior is obtained for $(R,S) = (10,1)$. The following important observations can be made. (i) The electric field does not affect the emulsion viscosity (i.e., $\eta^{(0)}_{\text{eff}} = \eta^{(0)}_{\text{eff},T}$) for $\phi_t = 0, \pi/2$, and π. (ii) The effect of the electric field in augmenting or reducing the emulsion viscosity is maximum for $\phi_t = \pi/4$ and $3\pi/4$. This is due to the fact that for these two tilt angles the EHD straining flow affects the straining component of shear flow most dominantly. With an increase in Mason number, the strength of the electric field relative to the viscous stress increases and the electric field plays a more dominant role in determining the decrease or increase in emulsion viscosity.

To investigate the effect of viscosity ratio, we plot the variation of the normalized effective viscosity with the viscosity ratio in Fig. 4 for $(R,S) = (0.1,1)$. It is important to note that the tilted electric field has a significant effect on the emulsion viscosity when the viscosity ratio is small. In the limit $\lambda \to \infty$, all the curves approach the Einstein viscosity limit. Figure 4 shows that the applied electric field has no effect for $\lambda \to \infty$, irrespective of the electrical properties and tilt angle. This is due to the fact that the EHD flow is diminished for $\lambda \to \infty$ and the drops behave as rigid spheres that strongly resist the straining component of the imposed shear flow. Previous studies have shown that a dilute emulsion of spherical drops has an effective viscosity smaller than the Einstein viscosity limit when there is no applied electric field. However, Fig. 4 shows that the application of an electric field leads to an effective viscosity larger than the Einstein viscosity limit for $\phi_t = \pi/4$ and $M = 3$.

The presence of an electric field not only alters the effective shear viscosity but also induces normal stress differences $N_1^{(0)}$ and $N_2^{(0)}$ [refer to Eq. (42)]. For the special case of an electric field acting in the velocity gradient direction (i.e., $E_x = 0$ and $E_y = 1$), the expressions of $N_1^{(0)}$ and $N_2^{(0)}$ match with the results of Vlahovska [29]. It is important to note that the normal stress differences appear solely due to the electric field; imposed shear flow has no effect on the normal stress differences at the leading order. Note that the normal stress differences are independent of shear rate. The inverse of the shear rate is present in the expression of M, but we have already nondimensionalized N_1 and N_2 by $\mu_e G$. Thus, the dimensional normal stress differences are independent of shear rate. To investigate the pivotal role of the tilt angle, we substitute $E_x = \sin\phi_t$ and $E_y = \cos\phi_t$. We obtain that the dependence of $N_1^{(0)}$ on the tilt angle is $\cos(2\phi_t)$, while the dependence of $N_2^{(0)}$ on the tilt angle is $\sin^2(\phi_t)$. Thus the first normal stress difference vanishes for $\phi_t = \pi/4, 3\pi/4$ and reaches its maximum value for $\phi_t = 0, \pi/2, \pi$. In contrast, the second normal stress difference vanishes for $\phi_t = 0, \pi$ and reaches its maximum value for $\phi_t = \pi/2$. Most importantly, the sign of $N_1^{(0)}$ and $N_2^{(0)}$ is strongly influences by the R/S ratio and ϕ_t.

B. Effect of charge convection on the emulsion rheology

Now we investigate the effect of surface charge convection on the emulsion rheology, neglecting the shape deformation. After incorporating the $O(\mathrm{Re}_E)$ contribution, we obtain the effective viscosity as

$$\eta_{\mathrm{eff}} = \eta_{\mathrm{eff}}^{(0)} + \mathrm{Re}_E \eta_{\mathrm{eff}}^{(\mathrm{Re}_E)}. \tag{74}$$

The $O(\mathrm{Re}_E)$ correction term is given in Eq. (54). The dependence on the components of electric field (E_x and E_y) will be more apparent if we arrange $\eta_{\mathrm{eff}}^{(\mathrm{Re}_E)}$ in the form

$$\eta_{\mathrm{eff}}^{(\mathrm{Re}_E)} = \nu M(S-R)\left[\frac{l_1 E_x^2 + l_2 E_y^2 + l_3 E_x E_y \left(E_x^2 + E_y^2\right) M(S-R)}{3500(\lambda+1)^2(3R+4)(R+2)^5}\right], \tag{75}$$

where the terms l_1, l_2, and l_3 are known functions of R, S, and λ, which are mentioned in Appendix D. A closer look into the expression of $\eta_{\mathrm{eff}}^{(\mathrm{Re}_E)}$ reveals that the effects of the imposed shear flow and imposed electric field are coupled and $\eta_{\mathrm{eff}}^{(\mathrm{Re}_E)}$ vanishes for $M = 0$. Importantly, the surface charge convection alters the effective viscosity of the emulsion even when the applied electric field is directed in the direction of either the shear flow or velocity gradient. This is in contrast to the leading-order contribution of the applied electric field, which is nonzero only when $E_x E_y \neq 0$. Substituting $\phi_t = 0$ or $\phi_t = \pi/2$, we obtain that the $O(\mathrm{Re}_E)$ correction in effective stress $\mathrm{Re}_E \eta_{\mathrm{eff}}^{(\mathrm{Re}_E)}$ is independent of shear rate. Thus, in the case in which the applied electric field is acting in the direction of either the shear flow or velocity gradient, the emulsion behaves as a Newtonian fluid but with altered effective viscosity due to charge convection. However, $\mathrm{Re}_E \eta_{\mathrm{eff}}^{(\mathrm{Re}_E)}$ depends on the shear rate when $E_x E_y \neq 0$ and the drops and suspending medium are leaky dielectric fluids with $R \neq S$.

The variation of the normalized effective viscosity with the viscosity ratio is depicted in Fig. 5(a) for $(R,S) = (0.1,2)$. We show the effect of charge convection for $\phi_t = 0$ and $\phi_t = \pi/2$. The effect of charge convection is noteworthy when the viscosity ratio is small. In the limit $\lambda \to \infty$, the velocity at the drop surface vanishes, which yields the effective viscosity of a suspension of rigid spheres. All the curves in Fig. 5(a) approach the Einstein viscosity limit. Figure 5(a) also shows that the surface charge convection decreases (or increases) the effective viscosity for $\phi_t = 0$ (or $\phi_t = \pi/2$). This alteration in effective viscosity is due to the $O(\mathrm{Re}_E)$ modification of the flow, which is generated by the $O(\mathrm{Re}_E)$ electrical tangential stress at the drop interface. We show the variation of surface charge density $q_s(\theta,\phi) = q_s^{(0)} + \mathrm{Re}_E q_s^{(\mathrm{Re}_E)}$ [refer to Eqs. (32) and (48)] with ϕ at the plane of shear flow (i.e., $\theta = \pi/2$) for $\phi_t = 0$. Figure 5(b) shows that the distribution of q_s in the presence of charge convection (i.e., $\mathrm{Re}_E = 0.1$) is significantly different from that of q_s in

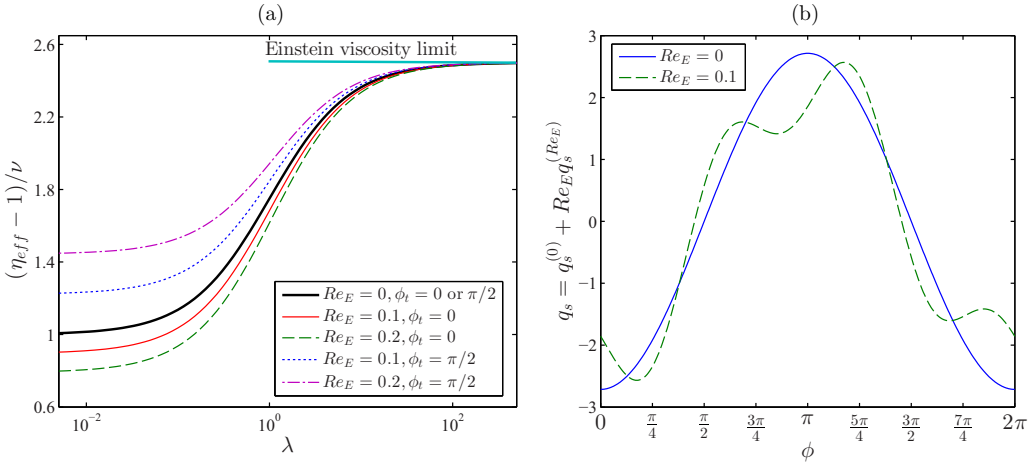

FIG. 5. (a) Variation of normalized effective shear viscosity with viscosity ratio. (b) Variation of surface charge density with ϕ for $\theta = \pi/2$ and $\phi_t = 0$. The other parameters are taken as $R = 0.1$, $S = 2$, and $M = 1$.

the absence of charge convection (i.e., $\mathrm{Re}_E = 0$). This altered charge distribution coupled with the tangential electric field generates an imbalance in tangential electric stress. The $O(\mathrm{Re}_E)$ imbalance in tangential electric stress induces EHD flow around the drop, which in turn affects the effective viscosity.

To investigate the effect of the tilt angle, we plot the variation of the normalized effective viscosity with the tilt angle in Fig. 6(a) for $(R,S) = (0.1,2)$ and in Fig. 6(b) for $(R,S) = (10,2)$. Both figures show that the surface charge convection can increase or decrease the effective viscosity depending on the value of the tilt angle. This is attributed to the fact that the tilt angle controls the direction of $O(\mathrm{Re}_E)$ EHD flow and thereby governs the effective viscosity.

Charge convection alters the normal stress differences. After incorporating the $O(\mathrm{Re}_E)$ contribution, we obtain the normal stress differences

$$N_1 = N_1^{(0)} + \mathrm{Re}_E N_1^{(\mathrm{Re}_E)}, \quad N_2 = N_2^{(0)} + \mathrm{Re}_E N_2^{(\mathrm{Re}_E)}. \tag{76}$$

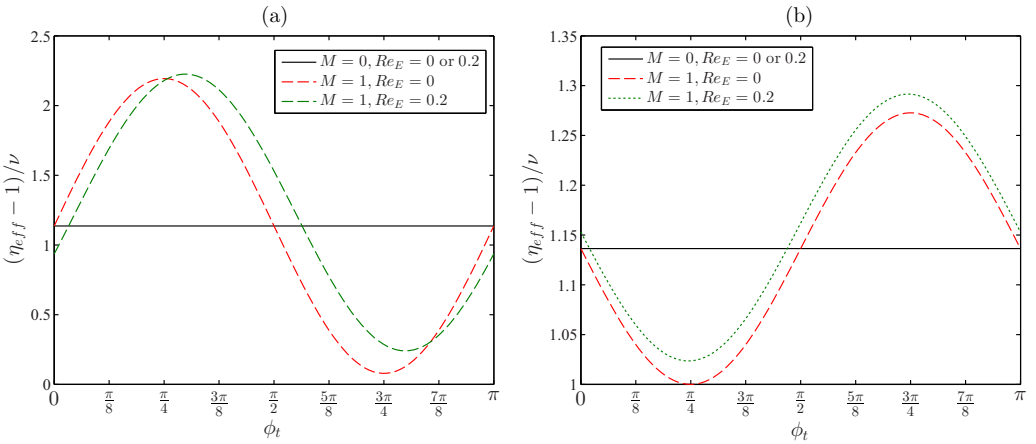

FIG. 6. Variation of normalized effective shear viscosity with tilt angle for (a) $R = 0.1$ and (b) $R = 10$. The other parameters are taken as $S = 2$ and $\lambda = 0.1$.

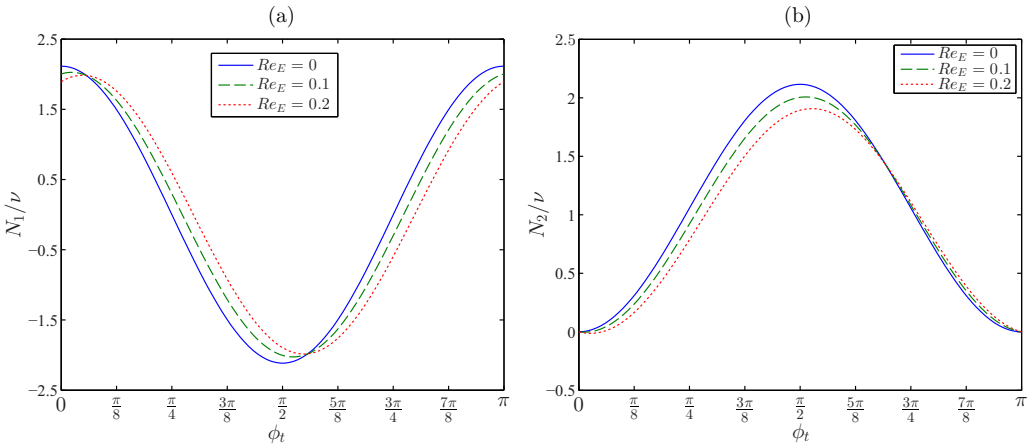

FIG. 7. (a) Variation of first normal stress with tilt angle. (b) Variation of second normal stress with tilt angle. The other parameters are taken as $M = 1$, $R = 0.1$, $S = 2$, and $\lambda = 0.1$.

The $O(\mathrm{Re}_E)$ corrections are given in Eqs. (56) and (57). The dependence on the components of the electric field (E_x and E_y) will be more apparent if we arrange $N_1^{(\mathrm{Re}_E)}$ and $N_2^{(\mathrm{Re}_E)}$ in the form

$$N_1^{(\mathrm{Re}_E)} = \nu M(S-R)\left[\frac{l_4\left(E_x^4 - E_y^4\right)M(S-R) + l_5 E_x E_y}{875(\lambda+1)^2(3R+4)(R+2)^5}\right],$$
$$N_2^{(\mathrm{Re}_E)} = \nu E_y M(S-R)\left[\frac{l_6 E_x + l_7 E_y\left(E_x^2 + E_y^2\right)M(S-R)}{1750(\lambda+1)^2(3R+4)(R+2)^5}\right], \tag{77}$$

where the terms l_4, l_5, l_6, and l_7 are known functions of R, S, and λ, which are mentioned in Appendix D. Note that the dimensional $O(\mathrm{Re}_E)$ correction in normal stress differences $\mu_e G\,\mathrm{Re}_E N_1^{(\mathrm{Re}_E)}$ and $\mu_e G\,\mathrm{Re}_E N_2^{(\mathrm{Re}_E)}$ depends on shear rate even when the applied electric field acts in the direction of the shear flow or velocity gradient. Variations of the normalized first and second normal stresses are shown in Figs. 7(a) and 7(b) for $(R,S) = (0.1,2)$. Surface charge convection leads to small changes in the first and second normal stresses that are attributed to the $O(\mathrm{Re}_E)$ EHD flow.

C. Effect of shape deformation on the emulsion rheology

Now we investigate the effect of shape deformation on the emulsion rheology, neglecting the surface charge convection. The expression of $f^{(Ca)}$ [given in Eq. (59)] suggest that the drop deforms to an ellipsoidal shape due to the combined effect of the shear flow and electric field. The sole effect of shear flow is to stretch the drop along the extension axis (i.e., orient the major axis of the ellipsoid at an angle $\pi/4$ with the direction of shear flow). On the other hand, the sole effect of the applied electric field is to orient the major axis of the ellipsoid parallel (perpendicular) to the applied electric field for $\Omega_T > 0$ ($\Omega_T < 0$). Simple calculation shows that in the combined presence of shear flow and an electric field the major axis of the ellipsoidal drop makes an angle ϕ_d with the flow direction, which can be obtained as

$$\phi_d = \frac{1}{2}\tan^{-1}\left(\frac{\hat{L}_{2,2}^{(Ca)}}{L_{2,2}^{(Ca)}}\right). \tag{78}$$

Thus, the applied electric field not only makes the drop ellipsoidal but also modulates the orientation of the drop shape. This altered shape and orientation are important contributing factors that will affect the resistance to imposed shear flow.

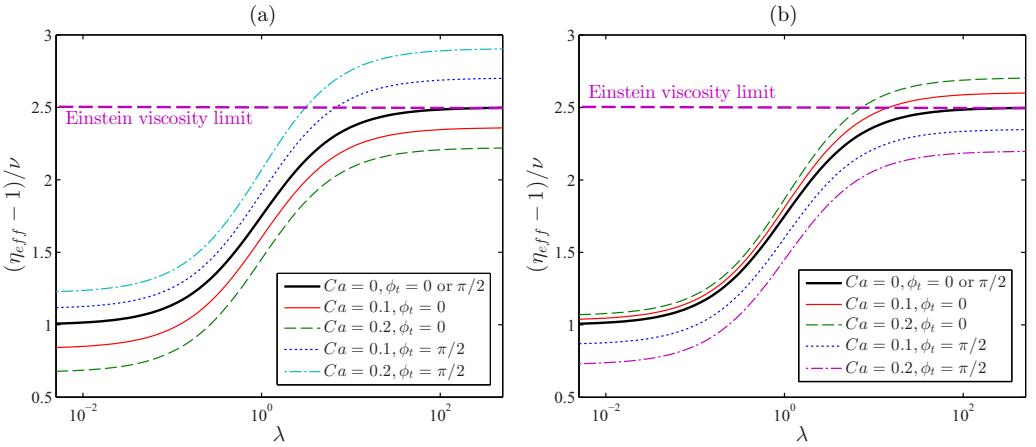

FIG. 8. Variation of normalized effective shear viscosity with viscosity ratio for (a) $R = 10$ and (b) $R = 0.1$. The other parameters are taken as $S = 1$ and $M = 1$.

After incorporating the $O(\mathrm{Ca})$ contribution, we obtain the effective viscosity

$$\eta_{\mathrm{eff}} = \eta_{\mathrm{eff}}^{(0)} + \mathrm{Ca}\eta_{\mathrm{eff}}^{(Ca)}. \tag{79}$$

The $O(\mathrm{Ca})$ correction is given in Eq. (69). The dependence on the components of the electric field (E_x and E_y) will be more apparent if we arrange $\eta_{\mathrm{eff}}^{(Ca)}$ in the form

$$\eta_{\mathrm{eff}}^{(Ca)} = \nu M\left[\frac{k_1E_x^2 + k_2E_y^2 + k_3E_xE_y\left(E_x^2+E_y^2\right)M(S-R)}{7000(\lambda+1)^3(R+2)^5}\right], \tag{80}$$

where the terms k_1, k_2, and k_3 are known functions of R, S, and λ, which are mentioned in Appendix E. A closer look into the expression of $\eta_{\mathrm{eff}}^{(Ca)}$ reveals that the effects of the imposed shear flow and imposed electric field are coupled and $\eta_{\mathrm{eff}}^{(Ca)}$ vanishes for $M = 0$, which was previously shown by Schowalter *et al.* [10]. Importantly, the shape deformation alters the effective viscosity of the emulsion even when the applied electric field is directed in the direction of either the shear flow or velocity gradient. This is in contrast to the leading-order contribution of the applied electric field that is nonzero only when $E_xE_y \neq 0$. Substituting $\phi_t = 0$ or $\phi_t = \pi/2$, we obtain that the $O(\mathrm{Ca})$ correction in effective stress $\mathrm{Ca}\eta_{\mathrm{eff}}^{(Ca)}$ is independent of shear rate. Thus, when the applied electric field is acting in the direction of either the shear flow or velocity gradient, the emulsion behaves as a Newtonian fluid but with altered effective viscosity due to shape deformation. However, $\mathrm{Ca}\eta_{\mathrm{eff}}^{(Ca)}$ depends on the shear rate when $E_xE_y \neq 0$ and the drops and suspending medium are leaky dielectric fluids with $R \neq S$.

The variation of normalized effective viscosity with the viscosity ratio is depicted in Fig. 8(a) considering $(R,S) = (10,1)$ for which $\Omega_T > 0$. We show the effect of shape deformation for $\phi_t = 0$ and $\phi_t = \pi/2$. When $\phi_t = 0$ the applied electric field tries to stretch the drop in the direction of shear flow, while the imposed shear flow tries to orient the drop at an angle $\pi/4$ with the direction of shear flow. The combined effect leads to $\phi_d < \pi/4$. Thus, the drop is aligned more towards the shear flow direction, which reduces the flow resistance and thereby decreases the effective viscosity as depicted in Fig. 8(a). In contrast, shape deformation increases the effective viscosity when $\phi_t = \pi/2$. This is due to the fact that when $\phi_t = \pi/2$ the applied electric field tries to stretch the drop in the direction of the velocity gradient, which leads to $\phi_d > \pi/4$. Thus, the drop is aligned more towards the velocity gradient direction, which increases the flow resistance and thereby increases the effective viscosity. Importantly, Fig. 8(a) also depicts that the high-viscosity limit (i.e., $\lambda \to \infty$) does not lead to Einstein viscosity in the presence of shape deformation (i.e., $\mathrm{Ca} > 0$). Figure 8(b) depicts

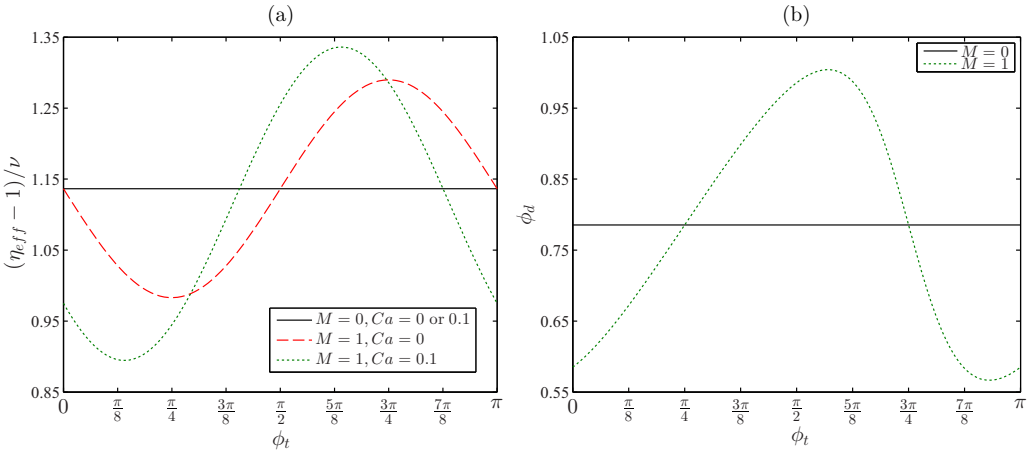

FIG. 9. (a) Variation of normalized effective shear viscosity with tilt angle. (b) Variation of drop inclination angle with tilt angle. The other parameters are taken as $R = 10$, $S = 1$, and $\lambda = 0.1$.

the variation of normalized effective viscosity with the viscosity ratio considering $(R,S) = (0.1,1)$ for which $\Omega_T < 0$. When $\phi_t = 0$ the applied electric field tries to stretch the drop in the direction of the velocity gradient. Thus, the combined effect of the shear flow and electric field leads to $\phi_d > \pi/4$. This increases the flow resistance and thereby increases the effective viscosity as depicted in Fig. 8(b). In contrast, shape deformation decreases the effective viscosity when $\phi_t = \pi/2$ as the combined effect of the shear flow and electric field leads to $\phi_d < \pi/4$.

To investigate the effect of the tilt angle, we plot the variation of normalized effective viscosity with the tilt angle in Fig. 9(a) for $(R,S) = (10,1)$. The corresponding variation in drop inclination angle is depicted in Fig. 9(b). Figure 9(a) shows that the tilt angle significantly affects the effective viscosity in the presence of shape deformation. This is attributed to the fact that the orientation angle of the ellipsoidal drop is strongly influenced by the tilt angle [refer to Fig. 9(b)]. The tilt angle modifies ϕ_d and subsequently the $O(\mathrm{Ca})$ flow. This $O(\mathrm{Ca})$ flow gives rise to shape-deformation-induced effective viscosity.

Shape deformation alters the normal stress differences. After incorporating the $O(\mathrm{Ca})$ contribution, we obtain the normal stress differences

$$N_1 = N_1^{(0)} + \mathrm{Ca}N_1^{(Ca)}, \quad N_2 = N_2^{(0)} + \mathrm{Ca}N_2^{(Ca)}. \tag{81}$$

The $O(\mathrm{Ca})$ corrections are given in Eqs. (71) and (72). The dependence on the components of the electric field (E_x and E_y) will be more apparent if we arrange $N_1^{(Ca)}$ and $N_2^{(Ca)}$ in the form

$$N_1^{(Ca)} = \nu\left[\frac{1}{40}\frac{(19\lambda+16)^2}{(\lambda+1)^2} + M\left\{\frac{k_4\left(E_x^4 - E_y^4\right)M(S-R) + k_5E_xE_y}{3500(\lambda+1)^3(R+2)^5}\right\}\right],$$
$$N_2^{(Ca)} = \nu\left[-\frac{1}{280}\frac{(19\lambda+16)(29\lambda^2+61\lambda+50)}{(\lambda+1)^3} + E_yM\left\{\frac{k_6E_x + k_7E_y\left(E_x^2+E_y^2\right)M(S-R)}{3500(\lambda+1)^3(R+2)^5}\right\}\right], \tag{82}$$

where the terms k_4, k_5, k_6, and k_7 are known functions of R, S, and λ, which are mentioned in Appendix E. Substituting $M = 0$ or $E_x = E_y = 0$ simplifies Eq. (82), which was previously obtained by Schowalter *et al.* [10]. Note that the dimensional $O(\mathrm{Ca})$ correction in normal stress differences $\mu_e G\,\mathrm{Ca}N_1^{(Ca)}$ and $\mu_e G\,\mathrm{Ca}N_2^{(Ca)}$ depends on shear rate even when the applied electric field acts in the direction of the shear flow or velocity gradient. Variations of the normalized first and

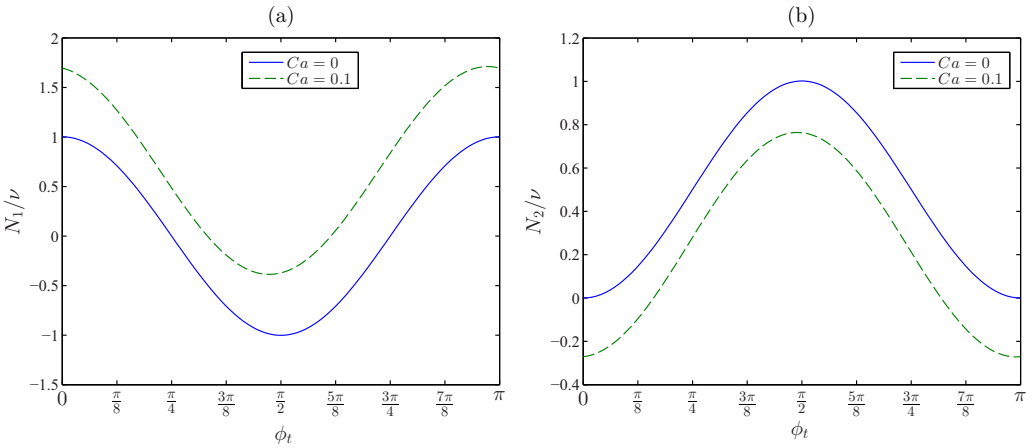

FIG. 10. (a) Variation of first normal stress with tilt angle. (b) Variation of second normal stress with tilt angle. The other parameters are taken as $M = 1$, $R = 0.1$, $S = 1$, and $\lambda = 0.1$.

second normal stresses are shown in Fig. 10(a) and 10(b) for $(R,S) = (0.1,1)$. Shape deformation leads to a significant change in the first and second normal stress differences, which is attributed to the $O(\mathrm{Ca})$ flow.

D. Electric torque and its effect on the emulsion stress

Up to now we have only discussed the importance of the electric field on the dynamical properties (effective viscosity and normal stress differences) that reflect the characteristics of the stresslet $\mathbf{\Sigma}^{(d)}$. Note that the stresslet is the symmetric and traceless part of the emulsion stress tensor. The antisymmetric part of the emulsion stress tensor, which is termed the rotlet $\boldsymbol{\mathcal{R}}^{(d)}$, can be expressed for a dilute emulsion as [39]

$$\boldsymbol{\mathcal{R}}^{(d)} = \frac{3\nu}{4\pi}\int_{S_d}\frac{1}{2}\left\{\left(\boldsymbol{\tau}_e^H\cdot\mathbf{n}\right)\mathbf{r} - \left[\left(\boldsymbol{\tau}_e^H\cdot\mathbf{n}\right)\mathbf{r}\right]^T\right\}dS_d. \tag{83}$$

The integral on the right-hand side of Eq. (83) can also be represented in terms of the hydrodynamic torque acting on the drop in the form [39]

$$\int_{S_d}\frac{1}{2}\left\{\left(\boldsymbol{\tau}_e^H\cdot\mathbf{n}\right)\mathbf{r} - \left[\left(\boldsymbol{\tau}_e^H\cdot\mathbf{n}\right)\mathbf{r}\right]^T\right\}dS_d = -\frac{1}{2}(\boldsymbol{\epsilon}\cdot\boldsymbol{\mathcal{T}}^H), \tag{84}$$

where $\boldsymbol{\epsilon}$ is the Levi-Cività tensor and $\boldsymbol{\mathcal{T}}^H$ is the hydrodynamic torque acting on the drop. Combining Eqs. (83) and (84), we obtain the rotlet

$$\boldsymbol{\mathcal{R}}^{(d)} = -\frac{3\nu}{8\pi}(\boldsymbol{\epsilon}\cdot\boldsymbol{\mathcal{T}}^H). \tag{85}$$

The genesis of hydrodynamic torque can be understood if we look into the torque balance equation, which states that the electric and hydrodynamic torques balance each other in the form [32]

$$\boldsymbol{\mathcal{T}}^H + M\boldsymbol{\mathcal{T}}^E = \mathbf{0}. \tag{86}$$

The hydrodynamic torque can be obtained as [39]

$$\boldsymbol{\mathcal{T}}^H = -8\pi\nabla(r^3\chi_{-2}), \tag{87}$$

where $\chi_{-2} = r^{-2}[C_{-2,0}P_{1,0} + C_{-2,1}P_{1,1}\cos\phi + \hat{C}_{-2,1}P_{1,1}\sin\phi]$ is a decaying solid harmonic. The electric torque can be obtained by integrating the electric traction vector in the form

$$\boldsymbol{\mathcal{T}}^{E} = \int_{\phi=0}^{2\pi}\int_{\theta=0}^{\pi} r_s \mathbf{e}_r \times \left(\boldsymbol{\tau}_e^{E}\cdot\mathbf{n}\right) r_s^2 \sin\theta d\theta d\phi. \tag{88}$$

Simple calculation shows that

$$\begin{aligned}
\boldsymbol{\mathcal{T}}^{H(0)} &= \boldsymbol{\mathcal{T}}^{E(0)} = \mathbf{0},\\
\boldsymbol{\mathcal{T}}^{H(\mathrm{Re}_E)} &= -M\boldsymbol{\mathcal{T}}^{E(\mathrm{Re}_E)} = \frac{4\pi M}{2+R}(\hat{Z}_{1,1}E_x - Z_{1,1}E_y)\mathbf{e}_z,\\
\boldsymbol{\mathcal{T}}^{H(Ca)} &= -M\boldsymbol{\mathcal{T}}^{E(Ca)}\\
&= -L_{2,2}^{(Ca)}\left(\frac{144}{5}\frac{\pi M E_x E_y (R-1)^2}{(R+2)^2}\right)\mathbf{e}_z + \hat{L}_{2,2}^{(Ca)}\left(\frac{72}{5}\frac{\pi M\left(E_x^2 - E_y^2\right)(R-1)^2}{(R+2)^2}\right)\mathbf{e}_z.
\end{aligned} \tag{89}$$

It is apparent from Eq. (89) that a uniform electric field exerts a nonzero electric torque (which translates to a hydrodynamic torque) in the presence of charge convection and shape deformation. This nonzero hydrodynamic torque results in a nonzero antisymmetric component of the emulsion stress tensor and effectively nonzero component of rotlet. The nonzero components of the rotlet are obtained as

$$\mathcal{R}_{xy}^{(d)} = -\mathcal{R}_{yx}^{(d)} = -\frac{3\nu}{8\pi}\left(\mathrm{Re}_E \mathcal{T}_z^{H(\mathrm{Re}_E)} + \mathrm{Ca}\mathcal{T}_z^{H(Ca)}\right), \tag{90}$$

where $\mathcal{T}_z^H$ is the z component of the hydrodynamic torque. Important to note here is that even though the electric torque does not influence the effective viscosity and normal stress differences, it does affect the rheology of the system by producing the antisymmetric component of the emulsion stress tensor.

V. CONCLUSION

In this paper we have studied the combined influence of a uniform electric field and simple shear flow on the effective shear rheology of a dilute emulsion comprised of neutrally buoyant, Newtonian, leaky dielectric drops suspended in an immiscible, Newtonian, leaky dielectric medium. In particular, we have explored the importance of the direction of a uniform electric field relative to the direction of shear flow. In the creeping flow limit, we have obtained an analytical solution for the effective stress of a dilute emulsion by performing regular perturbation analysis for small but finite values of Re_E and Ca. The effective shear viscosity and normal stress differences are obtained to $O(\nu)$, $O(\nu\,\mathrm{Re}_E)$, and $O(\nu\,\mathrm{Ca})$. Application of a uniform electric field generates electric torque due to charge convection and shape deformation, which in turn induces hydrodynamic torque on the drop. The electric torque leads to a nonzero antisymmetric part of the emulsion stress tensor. When the electric field is acting in the direction of the shear flow or velocity gradient, the dilute emulsion exhibits the following rheological characteristics [30]. (i) The effective viscosity is independent of shear rate. (ii) The leading-order EHD flow has no effect on the effective viscosity at $O(\nu)$; however, the charge convection and shape deformation contribute to the effective viscosity to $O(\nu\,\mathrm{Re}_E)$ and $O(\nu\,\mathrm{Ca})$, respectively. (iii) First and second normal stress differences are generated due to the leading-order EHD flow, charge convection, and shape deformation.

The physical picture gets dramatically altered when we consider the tilted electric field. The tilt angle has a significant effect on the effective viscosity and normal stress differences. The following important conclusions can be drawn from the present study.

(i) In the absence of charge convection and shape deformation, the EHD flow augments or resists the straining component of shear flow and thereby alters the effective viscosity and induces normal stress differences. The present analysis shows that the applied electric field alters the effective

viscosity only when $E_x E_y \neq 0$ and $R \neq S$. Most importantly, the applied electric field induces shear thinning or thickening behavior, depending on the values of ϕ_t and R/S. There is a critical Mason number M_{cr} for which the effective emulsion viscosity is the same as the viscosity of the suspending medium. Notably, the effective viscosity is larger (smaller) than the viscosity of the suspending medium for $M < M_{cr}$ ($M > M_{cr}$). The electric field has a significant effect on the effective viscosity when the drop is less viscous than the suspending medium; the effect of the electric field is diminished for $\lambda \to \infty$. The normal stress differences are independent of shear rate, but the signs of the first and second normal stress differences are strongly influenced by ϕ_t and R/S.

(ii) In the presence of charge convection, the distribution of surface charges generates an imbalance in tangential electric stress, which leads to an $O(\mathrm{Re}_E)$ modification of flow field and thereby a change in the effective viscosity and normal stress differences. Charge convection can augment or reduce the effective viscosity depending on the R/S ratio and ϕ_t. The charge-convection-induced alteration in effective viscosity depends on the shear rate only when $E_x E_y \neq 0$ and $R \neq S$.

(iii) In the presence of shape deformation, the $O(\mathrm{Ca})$ modification of the flow field alters the effect viscosity and normal stress differences. When the drop is inclined more towards the shear flow, the resistance to flow decreases and the shape deformation reduces the effective viscosity. When the drop is inclined in the velocity gradient direction, the resistance to flow increases and the shape deformation augments the effective viscosity. The shape-deformation-induced alteration in effective viscosity depends on the shear rate only when $E_x E_y \neq 0$ and $R \neq S$.

ACKNOWLEDGMENTS

S.M. is grateful to Dr. Aditya Bandopadhyay for insightful discussions at several stages of the mathematical calculations performed in this study. We thank the anonymous referee for an important suggestion.

APPENDIX A: EXPRESSION OF DIFFERENT TERMS IN THE LEADING-ORDER SOLUTION

The solid harmonics present in the leading-order flow field are obtained as

$$\begin{aligned}
p_2^{E(0)} &= \lambda r^2\big[A_{2,0}^{E(0)} P_{2,0} + A_{2,2}^{E(0)} \cos(2\phi) P_{2,2} + \hat{A}_{2,2}^{E(0)} \sin(2\phi) P_{2,2}\big],\\
\Phi_2^{E(0)} &= r^2\big[B_{2,0}^{E(0)} P_{2,0} + B_{2,2}^{E(0)} \cos(2\phi) P_{2,2} + \hat{B}_{2,2}^{E(0)} \sin(2\phi) P_{2,2}\big],\\
\Phi_{-3}^{E(0)} &= r^{-3}\big[B_{-3,0}^{E(0)} P_{2,0} + B_{-3,2}^{E(0)} \cos(2\phi) P_{2,2} + \hat{B}_{-3,2}^{E(0)} \sin(2\phi) P_{2,2}\big],\\
p_{-3}^{E(0)} &= r^{-3}\big[A_{-3,0}^{E(0)} P_{2,0} + A_{-3,2}^{E(0)} \cos(2\phi) P_{2,2} + \hat{A}_{-3,2}^{E(0)} \sin(2\phi) P_{2,2}\big],\\
p_2^{S(0)} &= \lambda r^2 \hat{A}_{2,2}^{S(0)} \sin(2\phi) P_{2,2}, \quad \Phi_2^{S(0)} = r^2 \hat{B}_{2,2}^{S(0)} \sin(2\phi) P_{2,2},\\
\chi_1^{S(0)} &= r\hat{C}_{1,0}^{S(0)} P_{1,0}, \quad p_{-3}^{E(0)} = r^{-3} \hat{A}_{-3,2}^{S(0)} \sin(2\phi) P_{2,2},\\
\Phi_{-3}^{S(0)} &= r^{-3} \hat{B}_{-3,2}^{S(0)} \sin(2\phi) P_{2,2},
\end{aligned} \tag{A1}$$

where the coefficients are obtained as

$$A_{2,0}^{E(0)} = -\frac{63}{10}\frac{M\big(E_x^2 + E_y^2\big)(R-S)}{(R+2)^2(\lambda+1)}, \quad B_{2,0}^{E(0)} = -\frac{A_{2,0}^{E(0)}}{14}, \quad A_{2,2}^{E(0)} = \frac{63}{20}\frac{M\big(E_x^2 - E_y^2\big)(R-S)}{(R+2)^2(\lambda+1)},$$

$$B_{2,2}^{E(0)} = -\frac{A_{2,2}^{E(0)}}{14}, \quad \hat{A}_{2,2}^{E(0)} = \frac{63}{10}\frac{M E_y E_x (R-S)}{(R+2)^2(\lambda+1)}, \quad \hat{B}_{2,2}^{E(0)} = -\frac{\hat{A}_{2,2}^{E(0)}}{14},$$

$$A^{E(0)}_{-3,0} = -\frac{9}{5}\frac{M\left(E_x^2+E_y^2\right)(R-S)}{(R+2)^2(\lambda+1)}, \quad B^{E(0)}_{-3,0} = \frac{A^{E(0)}_{-3,0}}{6}, \quad A^{E(0)}_{-3,2} = \frac{9}{10}\frac{M\left(E_x^2-E_y^2\right)(R-S)}{(R+2)^2(\lambda+1)},$$
$$B^{E(0)}_{-3,2} = \frac{A^{E(0)}_{-3,2}}{6}, \quad \hat{A}^{E(0)}_{-3,2} = \frac{9}{5}\frac{ME_yE_x(R-S)}{(R+2)^2(\lambda+1)}, \quad \hat{B}^{E(0)}_{-3,2} = \frac{\hat{A}^{E(0)}_{-3,2}}{6}, \quad \hat{A}^{S(0)}_{2,2} = \frac{7}{4(\lambda+1)},$$
$$\hat{B}^{S(0)}_{2,2} = -\frac{\hat{A}^{S(0)}_{2,2}}{14}, \quad \hat{C}^{S(0)}_{1,0} = -\frac{1}{2}, \quad \hat{A}^{S(0)}_{-3,2} = -\frac{1}{6}\frac{2+5\lambda}{\lambda+1}, \quad \hat{B}^{S(0)}_{-3,2} = -\frac{1}{12}\frac{\lambda}{\lambda+1}. \tag{A2}$$

APPENDIX B: EXPRESSION OF DIFFERENT TERMS IN THE $O(\mathrm{Re}_E)$ SOLUTION

The coefficients present on the right-hand side of $O(\mathrm{Re}_E)$ charging condition are obtained as

$$\begin{aligned}
Z_{1,1} &= c^{(0)}_{1,1}\left\{-\tfrac{1}{35}A^{E(0)}_{2,0} + \tfrac{6}{35}A^{E(0)}_{2,2}\right\} + \hat{c}^{(0)}_{1,1}\left\{-C^{S(0)}_{1,0} + \tfrac{6}{35}\left(\hat{A}^{E(0)}_{2,2} + \hat{A}^{S(0)}_{2,2}\right)\right\},\\
\hat{Z}_{1,1} &= c^{(0)}_{1,1}\left\{\tfrac{6}{35}\left(\hat{A}^{E(0)}_{2,2} + \hat{A}^{S(0)}_{2,2}\right) + C^{S(0)}_{1,0}\right\} + \hat{c}^{(0)}_{1,1}\left\{-\tfrac{1}{35}A^{E(0)}_{2,0} - \tfrac{6}{35}A^{E(0)}_{2,2}\right\},\\
Z_{3,1} &= c^{(0)}_{1,1}\left\{\tfrac{8}{105}A^{E(0)}_{2,0} - \tfrac{8}{105}A^{E(0)}_{2,2}\right\} - \tfrac{8}{105}\hat{c}^{(0)}_{1,1}\left\{\hat{A}^{E(0)}_{2,2} + \hat{A}^{S(0)}_{2,2}\right\},\\
\hat{Z}_{3,1} &= -\tfrac{8}{105}c^{(0)}_{1,1}\left\{\hat{A}^{E(0)}_{2,2} + \hat{A}^{S(0)}_{2,2}\right\} + \hat{c}^{(0)}_{1,1}\left\{\tfrac{8}{105}A^{E(0)}_{2,2} + \tfrac{8}{105}A^{E(0)}_{2,0}\right\},\\
Z_{3,3} &= \tfrac{4}{105}c^{(0)}_{1,1}\hat{A}^{E(0)}_{2,2} - \tfrac{4}{105}\hat{c}^{(0)}_{1,1}\left\{\hat{A}^{E(0)}_{2,2} + \hat{A}^{S(0)}_{2,2}\right\},\\
\hat{Z}_{3,3} &= \tfrac{4}{105}c^{(0)}_{1,1}\left\{\hat{A}^{E(0)}_{2,2} + \hat{A}^{S(0)}_{2,2}\right\} + \tfrac{4}{105}\hat{c}^{(0)}_{1,1}\hat{A}^{E(0)}_{2,2}.
\end{aligned} \tag{B1}$$

The coefficients present in the solid harmonics of the $O(\mathrm{Re}_E)$ flow field are obtained as

$$\begin{aligned}
A^{(\mathrm{Re}_E)}_{n,m} &= -\frac{(2n+3)M}{n(\lambda+1)(2n+1)}\left(ge^{(\mathrm{Re}_E)}_{n,m} - gi^{(\mathrm{Re}_E)}_{n,m}\right), \quad B^{(\mathrm{Re}_E)}_{n,m} = -\frac{A^{(\mathrm{Re}_E)}_{n,m}}{2(2n+3)},\\
A^{(\mathrm{Re}_E)}_{-n-1,m} &= \frac{n(2n-1)}{(2n+3)(n+1)}A^{(\mathrm{Re}_E)}_{n,m}, \quad B^{(\mathrm{Re}_E)}_{-n-1,m} = \frac{n}{2(2n+3)(n+1)}A^{(\mathrm{Re}_E)}_{n,m},\\
C^{(\mathrm{Re}_E)}_{n,m} &= \frac{M\left(he^{(\mathrm{Re}_E)}_{n,m} - hi^{(\mathrm{Re}_E)}_{n,m}\right)}{n(n+1)(n+\lambda n+2-\lambda)}, \quad C^{(\mathrm{Re}_E)}_{-n-1,m} = C^{(\mathrm{Re}_E)}_{n,m},\\
\hat{A}^{(\mathrm{Re}_E)}_{n,m} &= -\frac{(2n+3)M}{n(\lambda+1)(2n+1)}\left(\hat{g}e^{(\mathrm{Re}_E)}_{n,m} - \hat{g}i^{(\mathrm{Re}_E)}_{n,m}\right), \quad \hat{B}^{(\mathrm{Re}_E)}_{n,m} = -\frac{\hat{A}^{(\mathrm{Re}_E)}_{n,m}}{2(2n+3)},\\
\hat{A}^{(\mathrm{Re}_E)}_{-n-1,m} &= \frac{n(2n-1)}{(2n+3)(n+1)}\hat{A}^{(\mathrm{Re}_E)}_{n,m}, \quad \hat{B}^{(\mathrm{Re}_E)}_{-n-1,m} = \frac{n}{2(2n+3)(n+1)}\hat{A}^{(\mathrm{Re}_E)}_{n,m},\\
\hat{C}^{(\mathrm{Re}_E)}_{n,m} &= \frac{M\left(\hat{h}e^{(\mathrm{Re}_E)}_{n,m} - \hat{h}i^{(\mathrm{Re}_E)}_{n,m}\right)}{n(n+1)(n+\lambda n+2-\lambda)}, \quad \hat{C}^{(\mathrm{Re}_E)}_{-n-1,m} = \hat{C}^{(\mathrm{Re}_E)}_{n,m},
\end{aligned} \tag{B2}$$

where $gi^{(\mathrm{Re}_E)}_{n,m}$, $\hat{g}i^{(\mathrm{Re}_E)}_{n,m}$, $ge^{(\mathrm{Re}_E)}_{n,m}$, $\hat{g}e^{(\mathrm{Re}_E)}_{n,m}$, $hi^{(\mathrm{Re}_E)}_{n,m}$, $\hat{h}i^{(\mathrm{Re}_E)}_{n,m}$, $he^{(\mathrm{Re}_E)}_{n,m}$ and $\hat{h}e^{(\mathrm{Re}_E)}_{n,m}$ can be obtained from the relations

$$\sum_{n=0}^{\infty}\sum_{m=0}^{n}\left(gi^{(\mathrm{Re}_E)}_{n,m}\cos m\phi + \hat{g}i^{(\mathrm{Re}_E)}_{n,m}\sin m\phi\right)P_{n,m} = \mathbf{r}\cdot\left\{\nabla\times\left(\mathbf{r}\times\mathbf{T}^{E(\mathrm{Re}_E)}_{i}\right)\right\}\Big|_{r=1},$$
$$\sum_{n=0}^{\infty}\sum_{m=0}^{n}\left(ge^{(\mathrm{Re}_E)}_{n,m}\cos m\phi + \hat{g}e^{(\mathrm{Re}_E)}_{n,m}\sin m\phi\right)P_{n,m} = \mathbf{r}\cdot\left\{\nabla\times\left(\mathbf{r}\times\mathbf{T}^{E(\mathrm{Re}_E)}_{e}\right)\right\}\Big|_{r=1},$$

$$\sum_{n=0}^{\infty}\sum_{m=0}^{n}\left(hi_{n,m}^{(\mathrm{Re}_E)}\cos m\phi+\hat{h}i_{n,m}^{(\mathrm{Re}_E)}\sin m\phi\right)P_{n,m}=\mathbf{r}\cdot\left\{\nabla\times\mathbf{T}_i^{E(\mathrm{Re}_E)}\right\}\big|_{r=1},$$
$$\sum_{n=0}^{\infty}\sum_{m=0}^{n}\left(he_{n,m}^{(\mathrm{Re}_E)}\cos m\phi+\hat{h}e_{n,m}^{(\mathrm{Re}_E)}\sin m\phi\right)P_{n,m}=\mathbf{r}\cdot\left\{\nabla\times\mathbf{T}_e^{E(\mathrm{Re}_E)}\right\}\big|_{r=1}. \tag{B3}$$

Here $\mathbf{T}_i^{E(\mathrm{Re}_E)}$ and $\mathbf{T}_e^{E(\mathrm{Re}_E)}$ are the $O(\mathrm{Re}_E)$ electric traction vectors of the form

$$\begin{aligned}\mathbf{T}_i^{E(\mathrm{Re}_E)}=S\big[&\big\{E_{i,r}^{(0)}E_{i,r}^{(\mathrm{Re}_E)}-\tfrac{1}{2}\big(2E_{i,r}^{(0)}E_{i,r}^{(\mathrm{Re}_E)}+2E_{i,\theta}^{(0)}E_{i,\theta}^{(\mathrm{Re}_E)}+2E_{i,\phi}^{(0)}E_{i,\phi}^{(\mathrm{Re}_E)}\big)\big\}\mathbf{e}_r\\&+\big\{\big(E_{i,r}^{(0)}E_{i,\theta}^{(\mathrm{Re}_E)}+E_{i,r}^{(\mathrm{Re}_E)}E_{i,\theta}^{(0)}\big)\big\}\mathbf{e}_\theta+\big\{\big(E_{i,r}^{(0)}E_{i,\phi}^{(\mathrm{Re}_E)}+E_{i,r}^{(\mathrm{Re}_E)}E_{i,\phi}^{(0)}\big)\big\}\mathbf{e}_\phi\big]\end{aligned} \tag{B4}$$

and

$$\begin{aligned}\mathbf{T}_e^{E(\mathrm{Re}_E)}=\big[&\big\{E_{e,r}^{(0)}E_{e,r}^{(\mathrm{Re}_E)}-\tfrac{1}{2}\big(2E_{e,r}^{(0)}E_{e,r}^{(\mathrm{Re}_E)}+2E_{e,\theta}^{(0)}E_{e,\theta}^{(\mathrm{Re}_E)}+2E_{e,\phi}^{(0)}E_{e,\phi}^{(\mathrm{Re}_E)}\big)\big\}\mathbf{e}_r\\&+\big\{\big(E_{e,r}^{(0)}E_{e,\theta}^{(\mathrm{Re}_E)}+E_{e,r}^{(\mathrm{Re}_E)}E_{e,\theta}^{(0)}\big)\big\}\mathbf{e}_\theta+\big\{\big(E_{e,r}^{(0)}E_{e,\phi}^{(\mathrm{Re}_E)}+E_{e,r}^{(\mathrm{Re}_E)}E_{e,\phi}^{(0)}\big)\big\}\mathbf{e}_\phi\big].\end{aligned} \tag{B5}$$

APPENDIX C: EXPRESSION OF DIFFERENT TERMS IN THE $O(\mathrm{Ca})$ SOLUTION

The coefficients present in the $O(\mathrm{Ca})$ electric potential are obtained as

$$\begin{aligned}a_{1,1}^{(Ca)}&=\frac{9}{5}\frac{R-1}{(R+2)^2}\big[E_x\big(L_{2,0}^{(Ca)}-6L_{2,2}^{(Ca)}\big)-6\hat{L}_{2,2}^{(Ca)}E_y\big],\\
\hat{a}_{1,1}^{(Ca)}&=\frac{9}{5}\frac{R-1}{(2+R)^2}\big[E_y\big(L_{2,0}^{(Ca)}+6L_{2,2}^{(Ca)}\big)-6\hat{L}_{2,2}^{(Ca)}E_x\big],\\
b_{-2,1}^{(Ca)}&=\frac{1}{3}(1-R)a_{1,1}^{(Ca)},\quad \hat{b}_{-2,1}^{(Ca)}=\frac{1}{3}(1-R)\hat{a}_{1,1}^{(Ca)},\\
b_{-4,1}^{(Ca)}&=\frac{3}{5}\left(\frac{R-1}{2+R}\right)\big[\big(-L_{2,2}^{(Ca)}+L_{2,0}^{(Ca)}\big)E_x-\hat{L}_{2,2}^{(Ca)}E_y\big],\\
\hat{b}_{-4,1}^{(Ca)}&=\frac{3}{5}\left(\frac{R-1}{2+R}\right)\big[\big(L_{2,2}^{(Ca)}+L_{2,0}^{(Ca)}\big)E_y-\hat{L}_{2,2}^{(Ca)}E_x\big],\\
b_{-4,3}^{(Ca)}&=\frac{3}{10}\left(\frac{R-1}{2+R}\right)\big(-\hat{L}_{2,2}^{(Ca)}E_y+L_{2,2}^{(Ca)}E_x\big),\\
\hat{b}_{-4,3}^{(Ca)}&=\frac{3}{10}\left(\frac{R-1}{2+R}\right)\big(L_{2,2}^{(Ca)}E_y+\hat{L}_{2,2}^{(Ca)}E_x\big).\end{aligned} \tag{C1}$$

APPENDIX D: EXPRESSION OF DIFFERENT KNOWN FUNCTIONS IN EQS. (75) AND (77)

The expressions of l_1–l_7 are obtained as

$$\begin{aligned}l_1=&\,45(R+2)^2[315R^2\lambda-386R^2-124RS-630R\lambda S-210R\lambda\\&-1620R-1360-840\lambda-80S-840S\lambda],\\
l_2=&-45(R+2)^2[315R^2\lambda+1016R^2-1136RS-210R\lambda+1200R\\&-630R\lambda S-840\lambda-1600S-840S\lambda-320],\end{aligned}$$

$$
\begin{aligned}
l_3 &= 1944[-80S - 54RS + 69R^2 + 40 + 130R],\\
l_4 &= 33\,534R^2 - 26\,244RS + 63\,180R - 38\,880S + 19\,440,\\
l_5 &= -4725(3R + 4)(R + 2)^2(\lambda + 1)(R - 2 - 2S),\\
l_6 &= 135(R + 2)^2[105R^2\lambda - 22R^2 - 70R\lambda - 68RS - 220R - 210R\lambda S\\
&\quad - 280S\lambda - 280\lambda - 80S - 240],\\
l_7 &= 67\,068R^2 + 126\,360R - 52\,488RS + 38\,880 - 77\,760S.
\end{aligned}
\tag{D1}
$$

APPENDIX E: EXPRESSION OF DIFFERENT KNOWN FUNCTIONS IN EQS. (80) AND (82)

The expressions of k_1–k_7 are obtained as

$$
\begin{aligned}
k_1 &= -135(R + 2)^2[90R^3 + 90\lambda^3R^3 + 260\lambda^2R^3 + 260R^3\lambda + 1314\lambda^2R^2 + 1624\lambda R^2 + 640R^2\\
&\quad + 342\lambda^3R^2 - 342\lambda^3RS + 2R + 651\lambda^2R + 263\lambda R - 1314\lambda^2RS + 414\lambda^3R - 1624RS\lambda\\
&\quad - 640RS - 272S + 180\lambda^3 - 1431S\lambda^2 - 684S\lambda^3 + 180 + 520\lambda^2 + 520\lambda - 1043S\lambda],\\
k_2 &= 45(R + 2)^2[290R^3 + 395\lambda^3R^3 + 1110\lambda^2R^3 + 1005R^3\lambda + 2841\lambda^2R^2 + 1176\lambda R^2 - 128R^2\\
&\quad + 1501\lambda^3R^2 - 1501\lambda^3RS + 1898R + 5943\lambda^2R + 5952\lambda R - 2841\lambda^2RS\\
&\quad + 1817\lambda^3R - 1176RS\lambda + 128RS - 2768S + 790\lambda^3 - 9273S\lambda^2 - 3002S\lambda^3\\
&\quad + 580 + 2220\lambda^2 + 2010\lambda - 8967S\lambda],\\
k_3 &= 972(-12 + 15R - 16\lambda + 13\lambda R)(5\lambda R^2 + 5R^2 + 9\lambda R + 6R - 19S\lambda + 5\lambda - 16S + 5),\\
k_4 &= 486(15R + 13\lambda R - 16\lambda - 12)(5\lambda + 5 - 19S\lambda - 16S + 5\lambda R^2 + 5R^2 + 9\lambda R + 6R),\\
k_5 &= 315(5\lambda + 5 - 19S\lambda - 16S + 5\lambda R^2 + 5R^2 + 9\lambda R + 6R)(\lambda + 1)(19\lambda + 16)(R + 2)^3,\\
k_6 &= -45(R + 2)^2[250R^3 + 555R^3\lambda + 145\lambda^3R^3 + 450\lambda^2R^3 + 551\lambda^3R^2 + 1952R^2\\
&\quad + 2649\lambda^2R^2 + 4158\lambda R^2 - 551\lambda^3RS - 4158SR\lambda + 357\lambda^2R + 667\lambda^3R\\
&\quad - 2649\lambda^2RS + 36\lambda R - 1952SR + 130R - 880S + 500 - 1701S\lambda + 290\lambda^3\\
&\quad - 1707\lambda^2S + 1110\lambda + 900\lambda^2 - 1102S\lambda^3],\\
k_7 &= 486(-12 + 15R - 16\lambda + 13\lambda R)(5\lambda R^2 + 5R^2 + 9\lambda R + 6R - 19S\lambda + 5\lambda - 16S + 5).
\end{aligned}
\tag{E1}
$$

[1] D. A. Edwards, H. Brenner, and D. T. Wasan, *Interfacial Transport Processes and Rheology* (Butterworth-Heinemann, Waltham, 1991).

[2] *Rheology of Complex Fluids*, edited by J. M. Krishnan, A. P. Deshpande, and P. B. S. Kumar (Springer, New York, 2010).

[3] A. Malkin and A. I. Isayev, *Rheology: Concepts, Methods, and Applications*, Second (ChemTec, Toronto, 2012).

[4] R. Bandyopadhyay, Novel experimentally observed phenomena in soft matter, Pramana **81**, 3 (2013).

[5] G. G. Fuller and J. Vermant, Complex fluid-fluid interfaces: Rheology and structure, Annu. Rev. Chem. Biomol. Eng. **3**, 519 (2012).

[6] H. A. Barnes, Rheology of emulsions—A review, Colloids Surf. A **91**, 89 (1994).

[7] S. K. Tadavani, J. R. Munroe, and A. Yethiraj, The effect of confinement on the electrohydrodynamic behavior of droplets in a microfluidic oil-in-oil emulsion, Soft Matter **12**, 9246 (2016).

[8] G. I. Taylor, The Viscosity of a fluid containing small drops of another fluid, Proc. R. Soc. London Ser. A **138**, 41 (1932).
[9] G. I. Taylor, The formation of emulsions in definable fields of flow, Proc. R. Soc. London Ser. A **146**, 501 (1934).
[10] W. R. Schowalter, C. E. Chaffey, and H. Brenner, Rheological behavior of a dilute emulsion, J. Colloid Interface Sci. **26**, 152 (1968).
[11] R. V. Raja, G. Subramanian, and D. L. Koch, Inertial effects on the rheology of a dilute emulsion, J. Fluid Mech. **646**, 255 (2010).
[12] G. Subramanian, D. L. Koch, J. Zhang, and C. Yang, The influence of the inertially dominated outer region on the rheology of a dilute dispersion of low-Reynolds-number drops or rigid particles, J. Fluid Mech. **674**, 307 (2011).
[13] J. M. Rallison, The stress in a dilute suspension of liquid spheres in a second-order fluid, J. Fluid Mech. **693**, 500 (2012).
[14] P. M. Vlahovska, M. Loewenberg, and J. Blawzdziewicz, Deformation of a surfactant-covered drop in a linear flow, Phys. Fluids **17**, 103103 (2005).
[15] P. M. Vlahovska, J. Bławzdziewicz, and M. Loewenberg, Small-deformation theory for a surfactant-covered drop in linear flows, J. Fluid Mech. **624**, 293 (2009).
[16] A. Ramachandran and L. G. Leal, The effect of interfacial slip on the rheology of a dilute emulsion of drops for small capillary numbers, J. Rheol. **56**, 1555 (2012).
[17] A. Ramachandran, K. Tsigklifis, A. Roy, and G. Leal, The effect of interfacial slip on the dynamics of a drop in flow: Part I. Stretching, relaxation, and breakup, J. Rheol. **56**, 45 (2012).
[18] S. A. Faroughi and C. Huber, A generalized equation for rheology of emulsions and suspensions of deformable particles subjected to simple shear at low Reynolds number, Rheol. Acta **54**, 85 (2015).
[19] R. Pal, Fundamental rheology of disperse systems based on single-particle mechanics, Fluids **1**, 40 (2016).
[20] R. Pal, Rheology of simple and multiple emulsions, Curr. Opin. Colloid Interface Sci. **16**, 41 (2011).
[21] X. D. Pan and G. H. McKinley, Characteristics of electrorheological responses in an emulsion system, J. Colloid Interface Sci. **195**, 101 (1997).
[22] J.-W. Ha and S.-M. Yang, Rheological responses of oil-in-oil emulsions in an electric field, J. Rheol. **44**, 235 (2000).
[23] J.-W. Ha, J.-H. Moon, and S.-M. Yang, Effect of nonionic surfactants on the electrorheology of emulsions, Korea-Aust. Rheol. J. **11**, 241 (1999).
[24] D. A. Saville, Electrohydrodynamics: The Taylor-Melcher leaky dielectric model, Annu. Rev. Fluid Mech. **29**, 27 (1997).
[25] S. Mählmann and D. T. Papageorgiou, Numerical study of electric field effects on the deformation of two-dimensional liquid drops in simple shear flow at arbitrary Reynolds number, J. Fluid Mech. **626**, 367 (2009).
[26] A. Fernández, Response of an emulsion of leaky dielectric drops immersed in a simple shear flow: Drops more conductive than the suspending fluid, Phys. Fluids **20**, 43303 (2008).
[27] A. Fernández, Response of an emulsion of leaky dielectric drops immersed in a simple shear flow: Drops less conductive than the suspending fluid, Phys. Fluids **20**, 43304 (2008).
[28] A. Fernández, Shear flow of an emulsion of drops less conductive than the suspending fluid immersed in an electric field by numerical simulation, Colloids Surf. A **338**, 68 (2009).
[29] P. M. Vlahovska, On the rheology of a dilute emulsion in a uniform electric field, J. Fluid Mech. **670**, 481 (2011).
[30] S. Mandal and S. Chakraborty, Effect of uniform electric field on the drop deformation in simple shear flow and emulsion shear rheology, Phys. Fluids **29**, 72109 (2017).
[31] A. Bandopadhyay, S. Mandal, N. K. Kishore, and S. Chakraborty, Uniform electric-field-induced lateral migration of a sedimenting drop, J. Fluid Mech. **792**, 553 (2016).
[32] S. Mandal, A. Bandopadhyay, and S. Chakraborty, The effect of uniform electric field on the cross-stream migration of a drop in plane Poiseuille flow, J. Fluid Mech. **809**, 726 (2016).
[33] G. Taylor, Studies in electrohydrodynamics. I. The circulation produced in a drop by electrical field, Proc. R. Soc. London Ser. A **291**, 159 (1966).

[34] J. R. Melcher, G. I. Taylor, T. R. Melcher, and G. I. Taylor, Electrohydrodynamics: A review of the role of interfacial shear stresses, Annu. Rev. Fluid Mech. **1**, 111 (1969).
[35] X. Xu and G. M. Homsy, The settling velocity and shape distortion of drops in a uniform electric field, J. Fluid Mech. **564**, 395 (2006).
[36] G. Hetsroni and S. Haber, The flow in and around a droplet or bubble submerged in an unbound arbitrary velocity field, Rheol. Acta **9**, 488 (1970).
[37] G. K. Batchelor, The stress system in a suspension of force-free particles, J. Fluid Mech. **41**, 545 (1970).
[38] D. Barthès-Biesel, *Microhydrodynamics and Complex Fluids* (CRC, Boca Raton, 2012).
[39] S. Kim and S. Karrila, *Microhydrodynamics: Principles and Selected Applications* (Butterworth-Heinemann, London, 1991).
[40] J. Happel and H. Brenner, *Low Reynolds Number Hydrodynamics* (Springer Netherlands, Dordrecht, 1981).
[41] R. B. Bird, R. C. Armstrong, and O. Hassager, *Dynamics of Polymeric Liquids, Volume 1: Fluid Mechanics*, 2nd ed. (Wiley, New York, 1987).
[42] J. M. Rallison, The deformation of small viscous drops and bubbles in shear flows, Annu. Rev. Fluid Mech. **16**, 45 (1984).
[43] J. Q. Feng, Electrohydrodynamic behaviour of a drop subjected to a steady uniform electric field at finite electric Reynolds number, Proc. R. Soc. A **455**, 2245 (1999).
[44] P. C.-H. Chan and L. G. Leal, The motion of a deformable drop in a second-order fluid, J. Fluid Mech. **92**, 131 (1979).
[45] G. K. Batchelor and J. T. Green, The determination of the bulk stress in a suspension of spherical particles to order c^2, J. Fluid Mech. **56**, 401 (1972).
[46] L. G. Leal, *Advanced Transport Phenomena* (Cambridge University Press, Cambridge, 2007).
[47] P. F. Salipante and P. M. Vlahovska, Electrohydrodynamics of drops in strong uniform dc electric fields, Phys. Fluids **22**, 112110 (2010).